A Study of Smart Materials for Roofbolts Application in the Mining Industry

by

Shumane Joseph Moema

A dissertation submitted in fulfilment of the requirements for the degree in Magister Technologiae in the Department of Engineering Metallurgy, Faculty of Engineering and the Built Environment, University of Johannesburg

Supervisor	**: Prof. Antoine F. Mulaba-Bafobiandi (University of Johannesburg)**
Co Supervisor	**: Mr Bob Paton (Mintek)**
Mentor	**: Mr Christo Hattingh (University of Johannesburg)**

Declaration

I Shumane Joseph Moema declare that this dissertation is my own, unaided work. It is being submitted for the Degree of Magister of Technologiae at the University of Johannesburg. It has not been submitted before for any degree or examination in any other University.

Joseph Shumane Moema

January 2005

Author's signature: _____.....date: 04 January 2005

Dedication

This dissertation is dedicated to my mother (Elizabeth Sesi Ditshego) and my beloved wife Rynett Noko Moema.

Thank you for all of your love, help and support that you have given me over the years. You have been a constant source of inspiration to me. Also, thank you for being my best friends.

How can I forget the only one Almighty God for the wisdom he gave me.

Summary

This dissertation details the research performed into the development of a smart material for roofbolt application in the mining industry. It describes the methodology and research done to design a smartbolt using a metastable austenitic stainless steel. A number of measuring devices were used to study the properties and structure of this smartbolt alloy. These devices include a Ferritescope and a Krautkramer USM 25 DAC ultrasonic sound velocity measuring instruments.

The dissertation details the development, processing, laboratory and field testing of the smartbolt alloy. The designed alloy was found to have much stronger work-hardening effect, causing it to have a relatively low ductility. Therefore, the threads on the roofbolts produced from this alloy were machined instead of thread rolled.

It was also found that the incubation strain of the smartbolt alloy to be <5% and that the microstructural transformation rate is high, thus enabling effective monitoring.

Magnetic and ultrasonic techniques were used to monitor the progress of the $\gamma \rightarrow \alpha'$ transformation in the smartbolt alloy loaded in uniaxial and biaxial tension. It was found that the von Mises effective strain criterion gives a reasonable correlation of transformation kinetics. Using the modelling method, it was found that the failure strains for the rock are not the same as those for the smartbolt alloy.

All the smartbolts installed in the haulage tunnel (level 94 of mineshaft) showed a pattern of increasing longitudinal ultrasonic velocity (load) with time. This was due to the fact that mining was taking place above the area (in level 93 of the mineshaft).

Acknowledgements

My Supervisors

Prof. Antoine F. Mulaba-Bafobiandi, my supervisor, for his guidance and advice on writing of this dissertation.

Mr Robert Paton, my co-supervisor, for being critical to my methodology, also being supportive, his advice and technical input.

Mr Christo Hattingh, my mentor, for his patience, concern and advice.

Technical Assistance

Mr Stephen Roberts, for his technical input on uniaxial modelling of the alloy.

Mr Jonathan Kerr, for his technical input on multiaxial modelling of the alloy.

Mr Chris Fletcher, assisting in the mechanical testing.

Mr Ainsley Selengoane, being helpful when doing the installation of Smartbolts.

Mr Simon Pikekele, for his assistance in monitoring the installed Smartbolts.

Mr Peter Tladi, also for his time in installation and monitoring of Smartbolts.

Other VIPs

Dr Jones Papo, for proof reading of my dissertation and also for his advice.

Mr Duncan Adams, for choosing the test site and use of their equipment.

Mr Sandor Petho, technical input, especially the mining geology.

Institutions

Mintek, for their sponsorship in this research project and for the use of their facilities at Advanced Materials Division.

Simrac, for organising a meeting with South Deep mine personnel.

South Deep Gold mine, for allowing us to use their south shafts as our testing site for this project.

Mittal Steel Vereeniging, for the production and processing of the Smartbolt material.

University of Johannesburg, Engineering Metallurgy Department for allowing me to visit my mentor and supervisor to discuss the project.

Table of Contents

List of Figures

List of Tables

List of Abbreviations

SS – stainless steel
MPa – Mega Pascal
UTS – ultimate tensile strength
α' - alpha martensite
γ - austenite
ε - epsilon martensite
bcc – body centred cubic
fcc – face centred cubic
hcp – hexagonal closed packed
M_s – martensite start temperature
M_{d30} – martensite deformation temperature
wt – weight
TRIP – transformation induced plasticity
kN – kiloNewtons
SIM – strain induced martensite
δ - delta ferrite
M_f – martensite finish temperature
ε_f – final elongation
RD – rolling direction
A_g – uniform elongation
NDE – non destructive evaluation
FOG – fall of ground
Fe-Cr-Mn – Ferro chrome manganese steel
FGM – functional graded material
EFPI - extrinsic fabry-perot interfero-metric
DTI – direct tension indicator
SHM – structural health monitoring
FBG – fibre bragg grating
HRA – hot rolled annealing

CHAPTER 1

1 INTRODUCTION

This research project is part of an overall research programme on Smart Structural Health Monitoring, Development of Strain Sensing/Monitoring Technology based on the use of Metastable Materials and the concept of integrated "Smart" Structures/Sensors. The structural health monitoring systems that are currently being developed around the world are mainly based on the utilisation of new sensor technology/capabilities. The materials used for the production of these sensors are commonly known as "smart" materials.

Within the framework of this project, strain/stress monitoring technology will be explored utilising metastable alloy steel or the so called Transformation Induced Plasticity (TRIP) steels. The "smartness" of the TRIP steel is due to the fact that upon straining, a crystal structure transformation occurs within the material: metastable austenite is transformed into martensite which, unlike the austenite state, is ferromagnetic. The transformation from austenite to martensite state does not, however, only occur in TRIP steels. Various austenitic stainless steels and some alloys of the Fe-Cr-Mn group (smartbolt alloy) also exhibit such transformation.

Rock reinforcement is frequently used in tunnel constructions to stabilize the rock mass around a tunnel. Rockbolts are reinforcement devices used to reinforce the rock mass such that the subsequent deformation of the tunnel due to further excavation can be resisted. For this purpose, sufficient holding capacity is desired to ensure that rockbolts function properly. For conventional rockbolt types, the holding capacity is provided primarily by the shear resistance at the element–rock interface, by means of chemical cementation or mechanical friction of expansion elements.

Consequently, rock strength is a major requirement to achieve sufficient holding capacity. However, most of the rocks are inherently weak tertiary soft rocks that include sandstone, shale and mudstone, which are prone to weathering. In addition to weathering, the strength of soft rocks is further reduced to the extent that these rocks cannot provide sufficient holding capacity.

When tunneling in soft rock, where inherently more reinforcement and support are deemed necessary, rockbolts may be prevented from achieving their intended function, as the rock may be unable to provide a sufficient holding capacity. This inability leads to even more difficulty in the construction of tunnels. Consequently, the construction time and related costs are substantially increased.

Afterward, this expandable metal anchor is embedded in the enlarged borehole with grout, serving as the internal fixture, and is connected either by a rigid steel bar or by several steel strands to the external fixture. Selecting either a steel bar or steel strands depends on the designated tensile loading.

The steel strands are typically chosen to ensure a greater tensile loading, typically greater than 300 kN. When tensioning of the bolt element before service is required, i.e. pre-tensioning, the shank is not grouted until after the pre-tensioning has been applied. In terms of the holding mechanism, these rockbolts types can be categorized as mechanically anchored rockbolts, grouted rockbolts, jet-grouted rockbolts and under-reamed rockbolts.

1.1 Problem Statement

Rockbolting is a prerequisite for providing roof support in mining operations. The problem of rock pressure becomes worse as mining becomes deeper. Most of the rockbolts designs are made from simple carbon steel. The related problems of uncertainty as to the quality of installation of grouted steel tendons for reinforcement of rock around tunnels and stope gullies, and the effect of rock deformation and repeated dynamic loading from seismic events on the integrity of even well installed tendons, have been long recognised both in South Africa and world-wide.

Stress/strain monitoring of load bearing structural components used in different branches of engineering and the assessment of damage and structural integrity using non-destructive methods constitute an important engineering problem due to cost and safety implications. The importance of this problem arise from the fact that the percentage of mining tunnels that are being operated beyond their safe design lives is ever increasing and yet, their usage may need to be retained for many more decades to come because of increasing replacement costs. The inspection/monitoring techniques currently used in the majority of engineering applications are time consuming, costly and often not reliable.

Support, which is adequate on installation, may be insufficient when loading conditions change. A smart rockbolt was therefore proposed that, when stressed underground, undergoes a microstructural transformation, the amount of which depends on the degree of plastic deformation. These properties can, in primarily be monitored, using a portable magnetic and ultrasonic instrument, respectively, to determine the change in loading conditions, and to warn of a possible overload condition. The smartbolt thus acts as a sensor for the determination of stresses in mine workings.

Also, the microstructural evolution and transformation characteristics of this "smarbolt" alloy, capable of carrying substantial load, and at the same time serving as a sensor for accumulated damage, has not been sufficiently or extensively investigated at this stage; therefore this has led to an initiation of this project. The bolt in an underground environment experiences both horizontal and vertical forces (tensile and shear stresses), therefore more research work needs to be done; specifically the effect of these forces on the bolt.

1.2 Original Project Aim

The primary objective of this project was to characterise a Smartbolt™ alloy that may be used as a strain monitor in rockbolt applications for the mining industry. A secondary objective was to investigate the use of ultrasonic method in measuring the sound velocity in an individual bolt, under laboratory and underground environments. A third objective is to obtain "warning guidelines" for the use of this technology, which can be used to determine critical safety aspects in specific areas of each, mine.

1.3 Methodology

A literature survey was conducted using Metadex (or Internet) to look at all the Transformation Induced Plasticity (TRIP) steels and some alloys of the Fe-Cr-Mn group that are currently being used as SMART structures/sensors.

Also, an extensive literature survey was conducted in order to gain a fairly comprehensive overview of the various materials, techniques, and phenomena that ought to have been encountered in the course of the project.

The development, processing, laboratory and underground testing of the smartbolt material were carried out. The following further metallurgical evaluations were performed on the smartbolt material:

- Ferrite content measurement on annealed material
- Detecting of magnetic response/ %ferromagnetism during tensile testing i.e. interrupted tensile testing
- Microstructure in the annealed and strained condition by optical microscopy
- Determining of mechanical properties (tensile) in annealed condition
- Modelling of the alloy in the uniaxial and multiaxial state of stress
- Calibrating of the prototype smartbolt in uniaxial loading
- Ultrasonic sound velocity measurement of the smartbolt alloy

For the underground testing (testing on the mine) of the smartbolt material, prototype roofbolts were machined according to SABS 1408 of 1987 (code 142037). The thread length was approximately 150mm in length. One hundred smartbolts were prepared for installation. However due to time constraints only thirty-four bolts were tested. The proposed test site used 20mm diameter by 2400mm long roofbolts. One set of fourteen smartbolts (2400mm x 20mm) were installed in shaft 1, level 94 west at number 2 haulage tunnel and the other set (twenty smartbolts) in level 94 haulage ramp.

All sets of smartbolts were cement bonded and mechanically anchored. A Krautkramer USM 25 DAC ultrasonic measuring instrument was used to measure the sound velocity of the installed smartbolts.

1.4 Structure of the Dissertation

This dissertation describes the entire process followed for the development of a smartbolt material that will assess/monitor the condition of mining roof support systems.

Chapter 2: This chapter serves as a general review of recent research on metastable austenitic stainless steels, TRIP (Transformation-Induced Plasticity) steels and smart materials that could be used as a strain monitor/sensors in the mining industry. It is not intended to describe all that is known about this class of steels, since this is an extensive field, and not everything is pertinent to this project. Also, a review of the past and recent existing methods of *in situ* stress measurement.

Chapter 3: This chapter is part 1 of literature reviews on the theory and mechanism behind rockbursts and rockfalls that occurs in almost all the South African underground mining industry. Also, it covers a list of relevant past and recent papers dealing with the rockburst and rockfall phenomenon.

Chapter 4: This chapter is part 2 of literature reviews on the other stainless steel material that has similar properties to the Smartbolt alloy. The use of austenitic stainless steels is complicated by the metastability (unstable) of the austenitic structure of most alloys. Their metastability leads to a martensitic transformation (usually non–magnetic → magnetic but not always); also a volume change is experienced.

Chapter 5: This chapter outlines the experimental technique followed in the development, processing, and laboratory characterisation of the Smartbolt material. Also, selection of test site, and installation and monitoring of prototype rockbolts

Chapter 6: This chapter outlines the results obtained and a discussion of all the work performed including modelling of smartbolt alloy under uniaxial and multiaxial loading conditions, construction of calibration curve and underground testing of the smartbolt material.

Chapter 7: It concludes this dissertation with a discussion of the work performed and success of the project with respect to its aim.

Chapter 8: This chapter briefly serves to summarise all reference material used.

CHAPTER 2.

2 Literature Survey

2.1 Introduction

This chapter serves as a general review of recent research on metastable austenitic stainless steels, TRIP (Transformation-Induced Plasticity) steels and smart materials to be used as a strain monitor/sensors in the mining industry. It is not intended to describe all that is known about this class of steels, since this is an extensive field, and not everything is pertinent to this project. Finally a summary of all the past and recent existing methods of *in situ* stress measurement is given.

2.2 Smart Materials (Smartbolt alloy)

Over the past few years, Mintek[1 2] has developed a metastable austenitic stainless steel (smartbolt alloy) which is thermodynamically unstable so that plastic straining induces a transformation from a non-magnetic phase (austenite) to a magnetic one (martensite). The Md temperature (the upper temperature at which transformation to martensite may be induced by deformation) of the alloy has been determined. The formation of martensite during strain increases the work-hardening rate to an extent that the measured mechanical properties of this alloy are almost identical to those of the current carbon steel rockbolt used in the mining industry.

Furthermore, being of a 12% Cr base, the inherent corrosion properties of this alloy are far superior to these currently used rockbolts and thus have the propensity for much longer life in moderately corrosive environments. Also, the new alloy is far cheaper than commercially available grades such as types 304 and 316 stainless steel. These two latter alloys do not have similar mechanical properties to the currently used rockbolt.

Chopra[3], conducted a study and found that a smart structure involves distributed actuators and sensors and one or more microprocessors that analyze the responses from the sensors and use integrated control theory to command the actuators to apply localized strains/displacements to alter system response. A smart structure has the capability to respond to a changing external environment, such as loads or shape change as well as to a changing internal environment, such as damage or failure. It incorporates smart material actuators that allow the alteration of system characteristics, such as stiffness or damping, as well as of system response, such as strain or shape in a controlled manner.

Thus, a smart structure involves four key elements: actuators, sensors, control strategies, and power conditioning electronics. Many types of actuators and sensors, such as piezoelectric materials, shape memory alloys, electrostrictive materials, magnetostrictive materials, electro- and magnetorheological fluids and fibre optics, are being considered for various applications.

These can be integrated with main load-carrying structures by surface bonding or embedding without causing any significant changes in the mass or structural stiffness of the system

Reddy[4] in his work discovered a smart functionally graded plate that consists of a plate made of a functionally gradient material (FGM) and actuators made of an active material. The active material, a layer or set of patches, is bonded on the metal-rich surface of the functionally graded plate. When the ceramic-rich surface of the substrate is subjected to thermo mechanical loadings, displacements, and stresses may be controlled, and the actuators with supplied electric power may suppress vibration amplitudes.

In the attempt towards a basic understanding of the new type of smart structural system, this study considers a benchmark problem, namely, the bending of a functionally graded rectangular plate with an attached piezoelectric actuator. The transfer matrix and asymptotic expansion techniques are employed to obtain a three-dimensional asymptotic solution. In numerical computations, the locally effective material properties of the functionally gradient material are estimated by the Mori-Tanaka scheme. The three-dimensional distributions of displacements and stresses for different volume fractions of the ceramic and metallic constituents could serve as benchmark results to assess approximate theories and numerical methods. (FGM: Monel/zirconia).

2.3 Methods of stress measurement

Stacey[5] conducted a literature survey of the existing methods of *in situ* stress measurements including an evaluation of the applicability of these methods in deep level gold mines. The majority of methods of *in situ* stress measurements, which are available, were immediately rejected as being inapplicable for the deep gold mines. Based on the review of the available methods of *in situ* stress measurement, and experience in stress measurement programmes using numerous techniques, the following have been identified as requirements for a reliable, cost effective technique for *in situ* stress measurement in deep gold mines:

- the technique must be undemanding on requirement for services and personnel provided by the mine
- the technique should be low cost with regard to all aspects, cost of preparation, cost of installation, cost of instrumentation, cost per measurement, and economical in terms of time requirements
- the technique should not be sensitive to high stress effects such as spalling and micro cracking of the rock
- the technique should preferably not require laboratory testing to determine the deformation properties of the rock or rock mass

A method of *in situ* stress measurement, based on the percussion drilling of a set of three overlapping boreholes, (see Figure 1) and back analysing the *in situ* stresses from the measured deformations in the borehole, has been developed in concept.

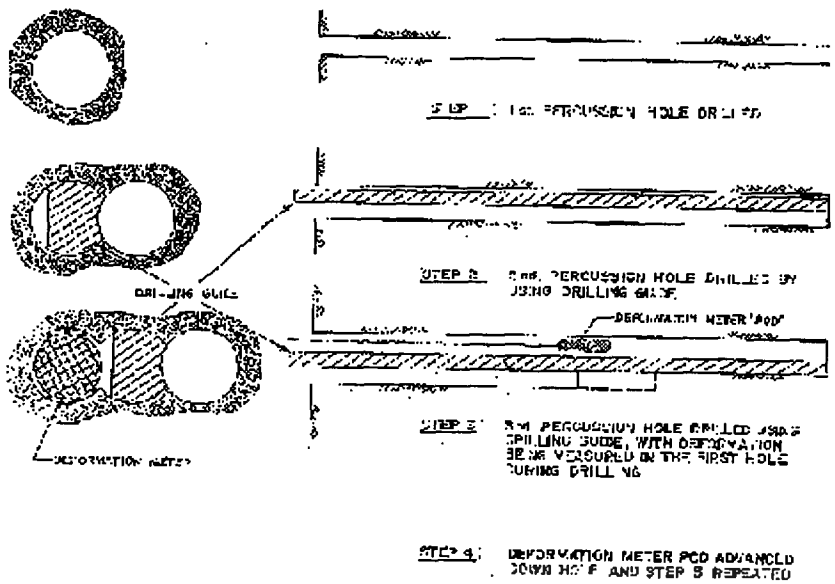

Figure 1. A method of in situ stress measurement, based on the percussion drilling of a set of three overlapping boreholes[5]

Gay[6] carried out a survey of 52 papers to identify methods, which could be of use for the determination of *in situ* stresses in coal mines. This survey showed that the majority of methods used to measure stress in coal are based on stress meters which are installed in boreholes drilled into the coal seam and then overcored by a larger diameter hole which results in the stresses acting on the sensor being relaxed. Measurement of the degree of relaxation allows an estimate to be made of the change in strain, which in turn, can be used to evaluate the original state of stress.

This study of stress measurement techniques, their advantages and disadvantages, has indicated a number of important requirements that are necessary for an *in situ* stress measuring technique that will give reliable results in coal mines. The technique should:

- be developed to work in South African coal fields
- be practical
- be sensitive to small change in stress
- allow many measurements to be made during a test
- and provide checks on the data obtained during the test

Canbulant and Jack[7] conducted a literature survey to investigate roof support mechanisms worldwide. The survey highlighted the fact that different roof support mechanisms have been used for various failure mechanisms. The literature review showed that three main rock reinforcement techniques have been used in coal mining; applications-beam building, suspension and rock strengthening. Extensive underground roof monitoring results showed that, in drill and blast sections, there is usually at least one pre-existing opening present in the roof virtually at the face which has an effect on the overall roof stability.

As a result of these openings in drill and blast sections, 42% of the total displacement takes place prior to the installation of support. The distance between the bolts is also an important factor for stability and safety. The analysis of FOG (fall of ground) fatalities showed that most of the FOG fatalities occurred due to relatively small pieces falling between the roofbolts. A design chart has been developed to determine the stability of the roof between the roofbolts and hence the appropriate spacing of bolts, see Figure 2. These design charts will assist rock engineers to decide on which support mechanism to use in specific strata.

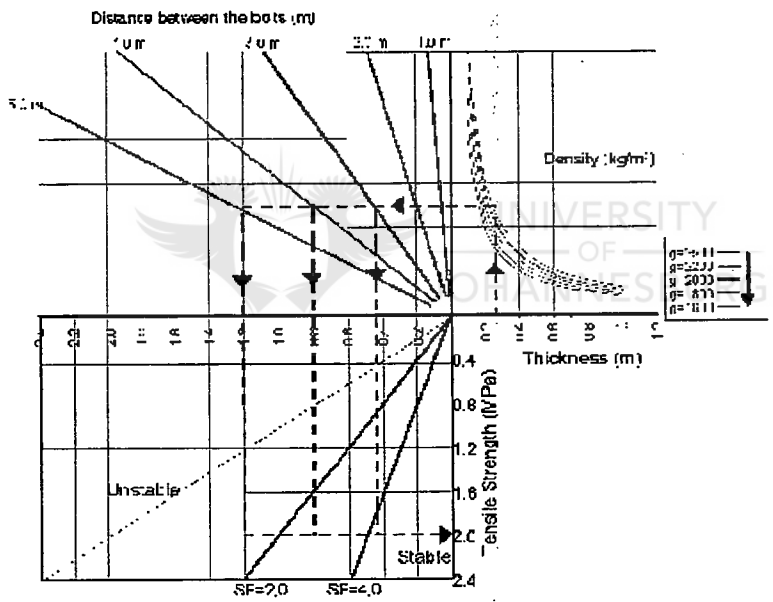

Figure 2. Design chart to determine the stability of roof strata between the bolts[7]

Stacey and Wesseloo[8] agreed that estimation of *in situ* stresses, using the existing *in situ* stress database and observations and interpretations of failure around openings, is a very important technique for developing an understanding of the *in situ* stress state. It is recommended that it should always be the first approach applied to obtain an indication of the *in situ* stress directions and magnitudes.

It should also be used as a check on the results of other methods of *in situ* stress measurement. This method should however, not be used in isolation, but with other methods to build an understanding of the stress regime.

Leng and Asundi[9] state that the real-time non-destructive evaluation (NDE) technologies of engineering structures are very important to assess the performance of in-service structures. It is very difficult to carry out on-line structural integrity monitoring by using classical NDE methods. Fiber optic sensors in smart structures provide a unique opportunity to monitor in real time the structural health status by using embedded sensors. This work examines the possibility of extrinsic Fabry-Perot interfero-metric (EFPI) and fiber Bragg grating (FBG) sensors for NDE of composite and aluminium structures. The 3-point bending experiments of composite laminates and aluminium plates with and without damages by using the EFPI and FBG sensors are performed, respectively.

The experimental results show that the flexural strain of damaged structures is much higher when compared with relevant undamaged structures under the same bending load by using both EFPI and FBG sensors. Furthermore, an excellent accordance was found between the results of the 3-point bending tests by using surface-mounted EFPI and FBG sensors

Murayama, Kageyama, Naruse, Shimada and Uzawa[10] stated that the purpose of structural health monitoring (SHM) is to lead a structure to be safer at a lower cost. In SHM, it is important to evaluate the actual state of the structure. Recently, fibre-optic sensors have been developed actively, and one can measure nearly all of the physical measurements of interest by them. Since they also have excellent characteristics such as high sensitivity, immunity from electromagnetic interference, good mechanical characteristics and distributed configuration, they have been applied to "smart structures."

Capability of quasi or fully distributed sensing is especially the significant advantage compared to conventional sensors. The authors have applied the fibre-optic distributed sensors to SHM in the field and have developed integrated systems with the fibre-optic sensors and CAD/CAE (computer aided design/computer aided engineering) for two large composite structures. These systems could give useful information on the structural state, such as deformation and temperature during/after manufacture

Stress Indicators, INC[11], has developed a DTI SmartBolts™ (Direct Tension Indicating Fasteners) which is based upon the response of an optical micro indicator element to the deflection of one internal portion of a fastener relative to another as the fastener elongates under tensile loading. This miniscule relative movement is transformed by patented DTI optical micro indicators into a dramatic and reproducible colour change.

Standard grade DTI SmartBolts™ provides an eye-catching bright indication of a loose or under tension condition. The bright red-orange indication of a loose fastener will gradually darken when tightening until it is a deep black at design tension. The amount of under-tension on fasteners may be readily estimated from the colour of the indicator. Precision grade DTI SmartBolt™ has been engineered to maximise indicator sensitivity and to position this maximum sensitivity and response at the fully tightened or high end of the tension range. The bright yellow indicator begins to turn colour at 70% of proof load, a grass green colour at design tension typically 90% of proof and has completely turned to a deep blue-black at 100% of proof load. This bolt is recommended by the US Bureau of mines to be used as mine roof bolts in the mining environment.

2.4 Methods of underground monitoring

There are a number of devices available with which roof deflection can be measured to supply prior warning of roof falls. They range from very accurate magnetic extensometers (very expensive) to more crude home made devices (less expensive). These devices are presented in the following sections:

2.4.1 Sonic extensometer

This method entails drilling long holes (typically more than 5m) into the roof on the face and to install magnetic anchors (measurements points) into those at predetermined spacing. At the same time special roof bolts fitted with strain gauges are installed. As time goes by, and the mine roadway is developed further, the displacement between the anchors and the build up of load on the bolts are determined very accurately. These rock movement measurements are taken using a sonic extensometer[12]. This then yield information about where and when partings develop in the roof and which parts of roof bolts get loaded more. Following these measurements roof movement 'action levels' can be derived for a site. Design measurement requires mine resources in the form of trained engineer at the mine to supervise measurements, interpret results and implement changes. A typical design monitoring station is shown in Figure 3.

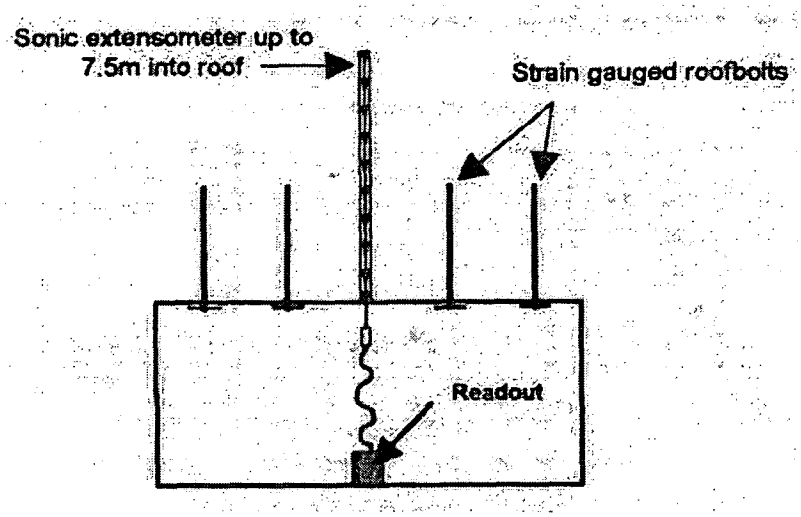

Figure 3. A typical roofbolted roadway monitoring station[12]

2.4.2 Telltales

Routine monitoring undertaken in rockbolted roadways by installing dual-height telltales[12] (Figure 4) which give a visual indication of roof displacement. They are designed so that the anchor positions are installed to a height beyond the likely extent of any expected roof movement. Each indicator has two coloured indicators graduated in millimetres, and corresponding to the predetermined action levels for roof movement within and above the rockbolted height. Telltale readings are taken by the district officials each shift and if excessive movement is detected, remedial action is taken. This remedial support action could be extra bolts, cable bolts or standing supports system. Typical South African coal mine roadway exceeds 4m in height resulting in difficulty in observing normal telltales at roof level.

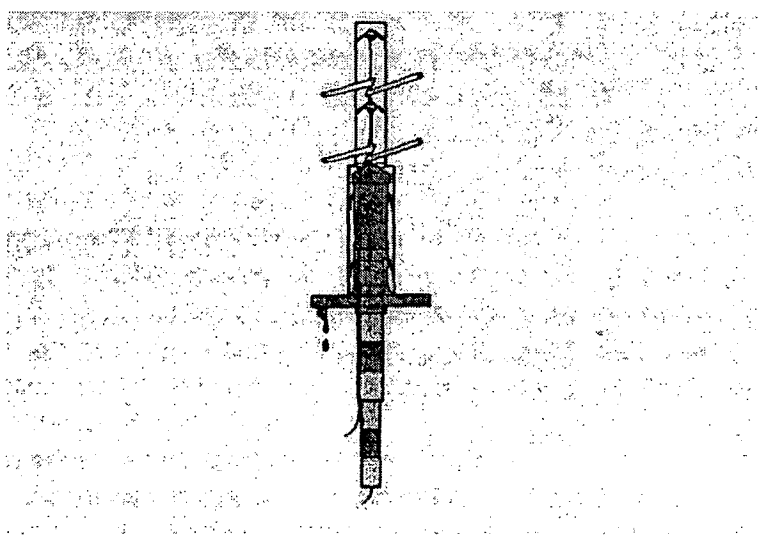

Figure 4. Dual-height telltale[12]

2.4.3 Acoustic Energy Meter (AEM)

The Acoustic Energy Meter[13] which measures the rate of decay of surface reverberation following an impact, was tested in a wide range of coal mine roof types and found to be sensitive to observed changes in roof conditions. It gives useful information on roof slip, progressive change in conditions with time and the effect of weathering, and major horizontal stress direction from measured directional variation in roof condition. The AEM is easy to use and to detect a variety of roof anomalies for a wide range of immediate roof conditions. There are however areas of uncertainty such as the maximum thickness of a detaching block which would still give an abnormal readings.

2.4.4 Ferritescope

The Ferritescope (Fischer model MP3 – see Figure 5) uses a two-point probe to form a closed magnetic circuit. The circuit is complete when the probe is in contact with the specimen and energized magnetic field. The voltage induced in the probe coil by this field is a direct measure of permeability and hence the amount of ferrite in the sample. The magnetic probe techniques allow only surface or limited volume measurements to be made. The manufacturers of the instrument (Fischer) have suggested the maximum depth of penetration is about 2.5 mm. This is a definite disadvantage of the method.

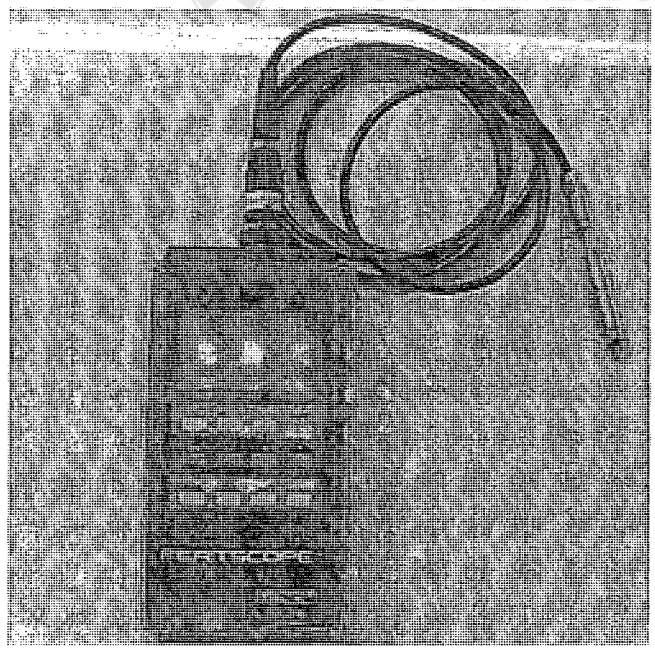

Figure 5. The Ferritescope (Fischer model MP3)

CHAPTER 3

3 Part 1: Rockbursts and Rockfalls

3.1 Introduction

This chapter is part 1 of literature reviews on the theory and mechanism behind rockbursts and rockfalls that occurs in almost all the South African underground mining industry. Also, covers a list of relevant past and recent papers dealing with the rockburst and rockfall mechanism.

3.2 Rockbursts

A rockburst is a dynamic failure, which is as a result of movement on a fault plane resulting in a violent release of energy into the surrounding rockmass often with disastrous consequences. These normally happen in the vicinity of structures, which due to the subsequent mining have modified the stresses, resulting in an instability of the rockmass. We also have what is termed a faceburst, which is voilent failure of the rock at a working face, due to high stresses causing the rock to fail and eject into the working place.

The purpose of this section is to summarise papers dealing with rockbursts in general. The chronological summary provides insights into the way in which research into the rockburst mechanism has grown over the years. Some ideas for modelling work are suggested.

Rockbursts are also describes as an explosive failures of rock which occurs when very high stress concentrations are induced around underground openings. The problem is particularly acute in deep level mining hard brittle rock condition. Figure 6 shows the damage resulting from a rockburst in an underground mine. The deep level gold mines from the Witwatersrand area in South Africa suffer from rockburst problems. Early work on rockbursts in South African gold mines was reported[14] and a summary of rockburst research up to 1966 was presented. A characteristics of almost all rockbursts is that they occur in highly stressed, brittle rock.

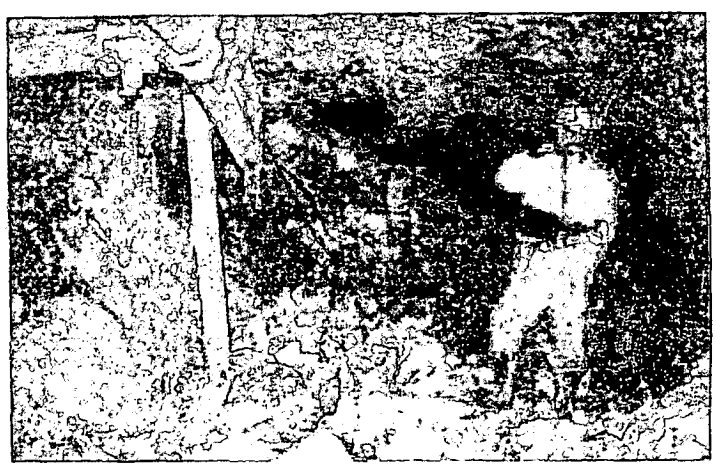

Figure 6. The results of a rockburst in an underground mine in brittle rock subject to very high stress[14]

Safety during construction and long term stability are factors, which have to be considered by the designers of excavations in rock. It is not unusual for these requirements to lead to a need for the installation of some form of rock support. In tunnelling, there is still an important role for steel sets and concrete lining in dealing with very poor ground but in slightly better ground, the use of combinations of rockbolts and shotcrete is common. The use of long untensioned grouted cables in underground mining has been a particularly important innovation, which has resulted in significant improvements in safety and mining costs in massive ore bodies. The use of untensioned grouted cables or reinforcing bars has also proved to be a very effective and economical technique in rock slope stabilisation. It is very effective in knitting the rock mass together and preventing the initiation of ravelling.

The strength of jointed rock masses is very dependent upon the interlocking between individual rock pieces. This interlocking is easily destroyed and careless blasting during excavation is one of the most common causes of underground excavation instability. The innocent rock mass is always blamed for insufficient instability that is actually the result of rough and careless blasting. Experience in projects in which carefully controlled blasting has been used generally shows that the amount of support can be reduced significantly and that the overall cost of excavation and support is lower than in the case of poorly blasted excavations. Examples of poor and good quality blasting in tunnels are illustrated in Figure 7 and Figure 8.

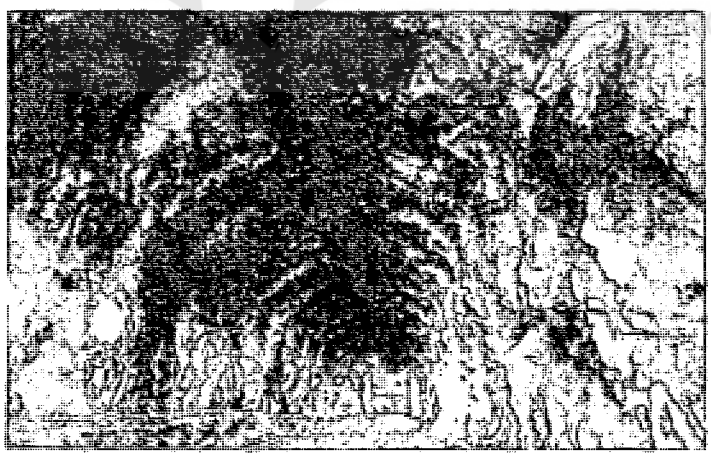

Figure 7. An example of poor blasting in a tunnel[14]

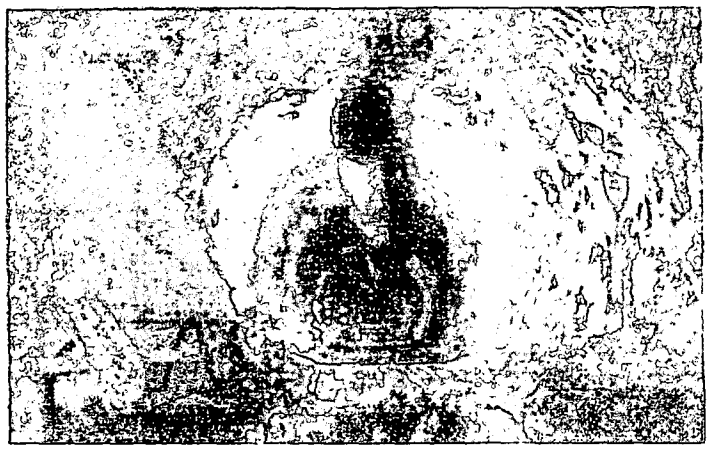

Figure 8. An example of good blasting in a tunnel[14]

Wood[15] was the first researcher to recognize mining induced seismicity on the Witwatersrand. His work concludes "... the tremors are semi–artificial in origin, and that the ultimate cause of them is to be found in the extraction of large amounts of rock ", and a suggested mechanism is "... slip by small amounts into positions of greater stability." In the discussion portion of the paper, the President of the Chemical, Metallurgical and Mining Society notes that the tremors cannot always be correlated with (pre–existing) planes of discontinuity; and cites an example of a mining induced fracture (with rockburst damage) of 100 m extent through a series of levels.

Allen[16], reported the observations of the effects of rockbursts and hanging wall behaviour at Robinson Deep in South Africa. Induced fracture planes in the hanging wall and/ or footwall are thought to be spaced more/less frequently as the face is more /less strong. Near remnant corners, the fractures are spaced more widely, because the face is not sufficiently strong to induce them, whereas near remnant centres, spacing is more dense. The paper concludes that, in order to have a burst, the surrounding rock mass must be sufficiently strong so that stress can be stored up until sudden failure occurs. A weaker rock mass would allow more frequent and safer fracturing. The suggestion is made that triangular remnants be mined so that their sides are concave to weaken the core more rapidly.

Weiss[17] discusses elasticity, plastic flow or creep, elastic hysteresis, temperature and humidity effects, rock strength, rupture conditions, rockbursts, measurements techniques in prediction of rockbursts. This is one of the early papers to realize plastic effects in gold mines. It notes that creep implies differential pressures which up to that time, hydrostatic conditions had been assumed even though evidence showed otherwise. Elastic hysteresis is suggested to be a secondary cause of many bursts, because bursts only release a portion of the stress, and as mining proceeds, complete dissipation of stress is not possible (hysteresis).

Stresses accumulate with time, causing subsequent bursts. Moisture and temperature gradient is thought to act on fissures in rock, reducing elasticity of rock, resulting in flaking and spitting of exposed faces. It is suggested that use of an air–and water–tight paint could reduce spitting and flaking. Seismic wave velocity is said to be a function of applied stressed. Areas of rock mass with lower wave velocity are therefore more highly stressed, and are of potential failure.

Morrison[18], suggests that the dome (elliptical shape around a stope) controls rock bursts. Sagging hanging walls are only outward indications of the development of a fractured zone and its related dome. It notes that the sizes of opening versus depth of mining are inter–related, i.e. shallow large excavation can experienced more rock bursts than a deeper but smaller excavation.

It notes that a grid system of pillar support, so as to shorten spans, is ineffective and worsens the situation. The stresses set up by such a system must ultimately overcome the resistance of individual domes in the process of building a single dome.

Spalding[19], work discusses general observation about rock bursts. It suggests that rocks, which consist of a single ingredient (e.g. quartz), are more likely to bursts than agglomerates. In homogeneities and varying grain sizes cause plastic flow and result in progressive failure. More homogenous rocks will tend to fail over a larger area and more violently when the elastic limit is reached.

Hill[20], noted a number of factors in relation to bursts that need to be investigated in order to determined their importance, namely. stoping method, face shapes, leads, percentage mining, spans, support types, closure amounts, closure rates, face advance rates depth of workings, and geological features. The paper concludes that face leads/lags should be avoided, long walling is better than scattered mining, acute angles of incidence should be avoided, dykes and faults have a pronounced effect on bursts incidence, and blasting can act as a trigger. Other questions remained unanswered.

Cook[21] summarizes research approach to rockbursts problem as a four-stage effort: (1) observation. (2) attack rational significance to documented experience and thereby develop hypotheses concerning certain aspects of rockbursts problem. (3) combine hypotheses to postulate a rockbursts mechanism consistent with observation. (4) design controlled experiments under ground to proposed mechanism, and eventually aim to minimize rockburst effects.

The paper summarises key observations, rock properties , elastic theory, and energy effects and concludes that the " existence or otherwise of the rockburst hazard depends on whether the geometrical rate at which energy must be released, is greater or smaller than the rate at which energy can be dissipated non-violently as the excavation is enlarged".

Rockbursts are thus postulated to be manifested as a release of that part of the energy generated by the elastic closure which is not absorbed in strain energy and is in excess of that which can be absorbed in fracturing of rock and in friction along fractures. With respect to de-stressing, of the face to alleviate rockbursts conditions, the authors claim that it has almost no effect, and base their argument on the type o seismic wave radiated during preconditioning (compressional) versus during an event (shear).

The argument is flawed, and one needs to look at the evidence of distressing, not at the type of wave radiated. In the discussion on the paper, Plewman suggests that two further breakthroughs are needed in order to understand more fully the rockbursts problem:1) a full understanding of in-situ fracturing processes and the behaviour of fractured materials, 2) an understanding of the dynamic loading processes and the behaviour of rock around stopes under dynamic loading.

Brink and O'Conner[22] conducted a research into the prediction of rockbursts at Western Deep Levels gold mine. For cases investigated, results show that seismic events within the local area monitored were preceded by an increased by an increased level of micro-seismicity, which concentrated in the zone of eventual failure. There was usually a short-lived marked drop in activity immediately prior to the event.

Salamon[23] outline a summary of progress made until 1983 in developing effective face support, good layout design, and control of convergence volume as ways of alleviating the rockbursts hazard. Mechanism: seismic energy released in a region is much less than energy released by mining (0.1% efficiency), which raises the question of what causes a rockbursts (clearly not correlated with ERR).

Salamon notes that a small mining step can cause a large rockbursts, which implies that either the rock mass must be discontinuous, or the rock must become an unstable material under certain loads. Suggests that alleviation of rockbursts can be accomplished through better layout design, reduction in stoping width, use of backfilling, partial extraction and improved support systems.

Cook[24], presented a conceptual model fracture zone (needed in order to understand origin of rockbursts) around a stope, based on practical, theoretical and experiment work. Three types of fractures are postulated: cleavage (tensile failure), inclined shear, and vertical shear fractures. Vertical fractures are suggested to be more likely candidates for the origin of the rockbursts. Cook suggests a cycle of cleavage, accompanied by dilatancy, which increases confining stresses and stops cleavage, followed by inclined shear (after sufficient build up of confinement), which reduces confining stresses, followed by cleavage again. This process continues with advance of the stope face. The inclined shear direction coincides with Mohr-Coulomb planes of failure. The vertical shear fractures develop along the line of maximum stress difference, on a plane through the stope face. Cleavage is not possible here because of confinement.

Gay[25] correlated seismicity with geology and mining in order to better understand origin of large mining-induced seismic events. Gay stresses the importance of faults and dykes-stiffer properties of dykes allows more energy to be stored up, and more chance of brittle failure. He mentions that the in situ stress field in the Klerksdorp area is such that large deviatoric stresses are present, capable of causing movement along faults and dykes. Mining activity disturbs this potentially unstable stress field, with the result that the generation of large events is quite possible in large possible in large volumes of rock.

Ortlepp[26] overviewed the rockburst problem in RSA, and compares with El Teniente mine in Chile. It suggests that the best way to understand rockburst is via seismic research. Such research and studies of rockbusrt damage should be used to develop guidelines (in Chile) for improved layouts and sequences to minimize the frequency of rockbursts, and for improved criteria for design of support to reduce damage to workings.

Knoll and Kuhnt[27] claim that rockburst can be divided into two types–mining rockburst associated with immediate mining activities, and tectonic rockburst associated with the tectonic conditions around the mine and large scale stress reditributions around the mine. Analysis of seismic records by spectral analysis shows that there are different scaling laws for the seismic moment and source radius for the two types rockbursts. It is proposed that, according to the seismologically indicated type of rockburst, appropriate measures can be taken to limit the effects of rockbursts in a mine.

Johnston and Einstein[28] conducted a survey of mining associated seismicity in a number of countries. An attempt is made to sort events into two types. Type I: seismicity linked directly to mining and geometry. Type II: seismicity occurring on faults, more similar to earthquakes. Six mechanism of failure are identified: (a) ore extruded because of high vertical stress from overburden, (b) roof collapse, (c) slip along faults, (d) fracture of intact rock ahead of advancing face, (e) fracture at the face from stress concentrations, (f) pillar bursting. Claim that (d), (e) and (f) produce rockbursts.

King[29] conducted a laboratory scale faults experiment, where 8 blocks connected by springs are driven to slide on a frictional surface. Suggest that frictional sliding may be chaotic. Also, rupture initiation points are not generally near maximum slip points

Ortlepp[30] elaborated on "rock-flour" of rhombic dodecahedral shape that forms part of the comminuted filling in shear fractures (visible under scanning electron microscope) in some samples. It suggests that this is evidence of shock rebound phenomena during a rockburst, because such shapes can only form by rapid unloading. Implication for rupture mechanism is that this evidence implies that the formation of a pristine fault by a shearing action is a more violent and less homogeneous process that was previously thought possible.

3.3 Rockfalls

A rockfall is caused by a gravitational force resulting in a fall of ground. It is a static failure, which can occur anywhere where there is not enough support to overcome the forces of gravity.

The problem of rockfall fatalities is arguably the most severe and persistent safety issue for the underground mining industry world-wide[31]. It was clearly established that rockfall risks can be divided into two specific types: the risk existing in the intense working areas near active faces and the risk present in the rest of the mine, including travel ways, declines, accesses, etc. Significant progress has been made in recent years, reducing rockfall injuries with improved mining practices near the active face. However, a remnant risk of rockfall injuries remains due to small rocks detaching from in between rockbolts.

The risk profile of rockfall fatalities in underground hard rock gold mines has also shifted in recent years, see Figure 9. Previous practices led to a majority of relatively small rockfalls causing fatalities near active faces, before the installation of ground support took place. More recently, fatal rockfalls have been larger and have a tendency to occur away from the face, in supported areas. As the risk of rockfalls is continually changing with changing mining practices, and the changing mining environment, it is essential to continue monitoring the causes of rockfalls.

Rockfalls in underground mines will continue to occur due to the complex and unpredictable nature of the geological environment in which mining activities take place. However, the use of Smartbolt technology should help to promote safety in the mining industry.

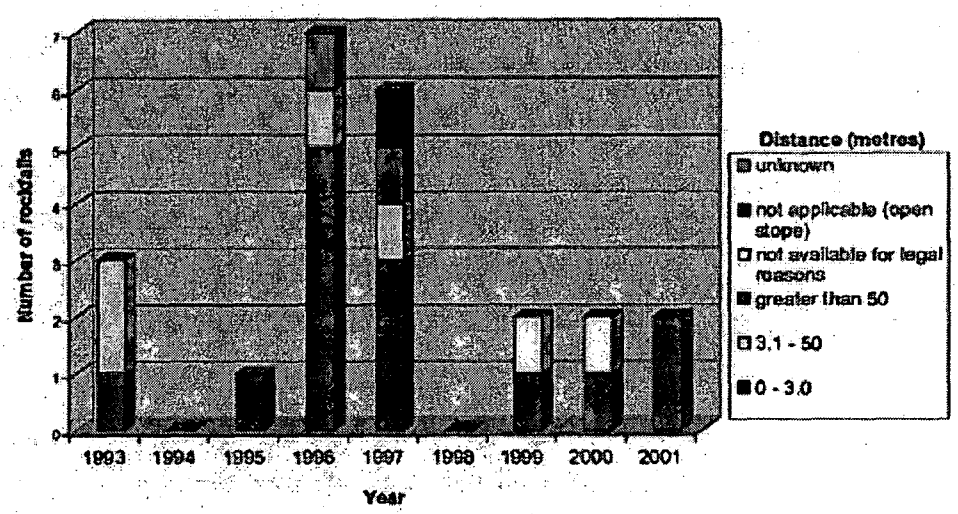

Figure 9. Distribution of rockfall fatalities according to the year of occurrence and the distance from active face[31]

Fatal accidents caused by gas explosions, rock falls, breaches of health and safety regulations, not to mention seismic actions, remain a grim reality for the local mine industry, resulting in the death of hundreds of miners each year. Accidents continue to occur in mines despite the new regulations issued by the Department of Minerals and Energy aimed at bringing down the number of incidents. It seems the blame lies squarely on poor legislation, and therefore the government needs to act fast to save mineworkers from possible accidents through speedy amendments to regulations.

Mining accidents were frequent until concerted and systematic efforts were made by industry, government and labour to improve safety[32]. Today fatality frequency rates (FFR), which measure fatalities per million hours worked, are at their lowest level ever for South African underground mines after nearly a decade of continuous improvement. South African surface operations have also shown a similar, though not as steady a downward trend (see Figure 10).

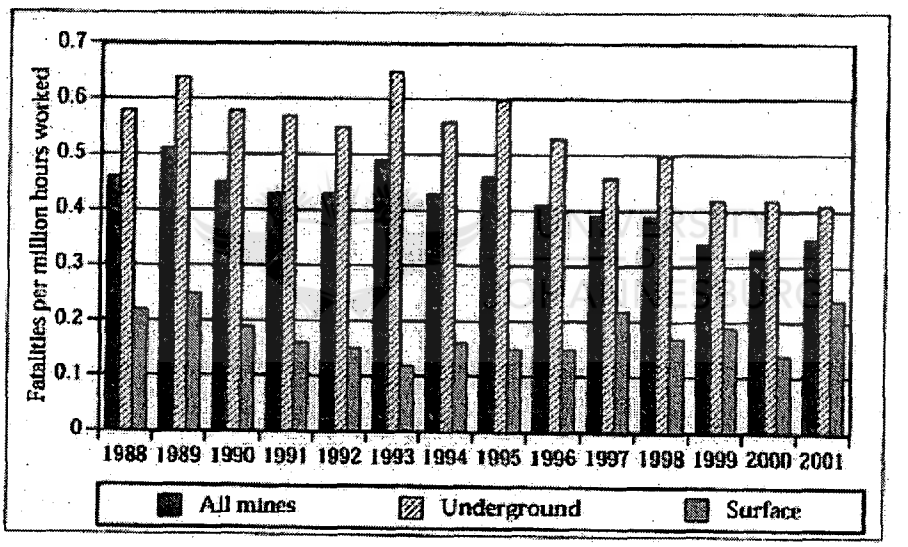

Figure 10. Fatality frequency rates – South African mines[32]

Comparing safety statistics comprising different proportions of underground and surface data can lead to erroneous conclusions when attempting benchmark safety performance. More useful information is gained by comparing surface operations with surface operations, and underground operations with underground operations. Since 78 per cent of hours worked on metalliferous mining (chrome, copper, gold, iron ore and platinum) are worked underground, the South African metalliferous mining industry is, in terms exposure to occupational, health and safety risks, predominantly an underground mining industry. The metalliferous mining industries in the United States and Australia on the other hand, are largely surface operations.

Surface operations have fewer hazards than underground operations, and the consequences of an accident are usually less severe. The safety performance of metalliferous mines in South Africa is however, approaching that of developed countries (see Figure 11).

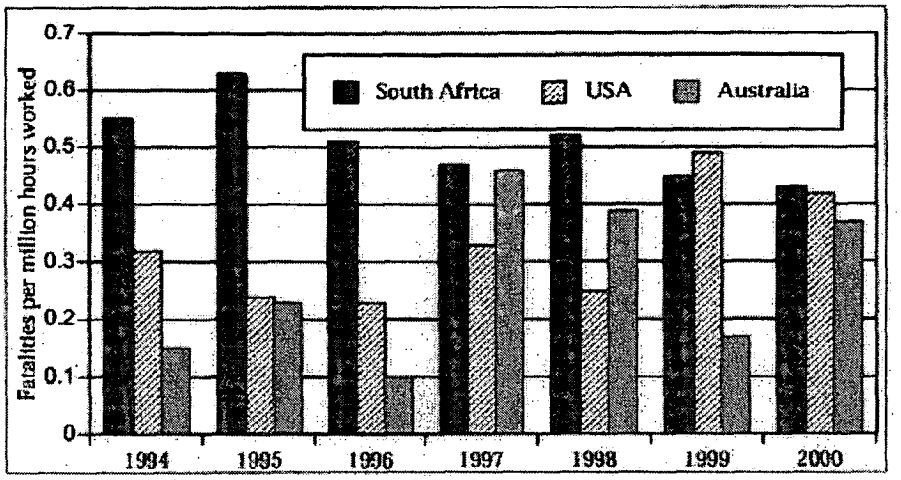

Figure 11. International comparison - fatality frequency rates on underground metalliferous mines[32]

Coal mines account for approximately 13 per cent of the total number of people employed in the mining industry. The FFR for coal mines (underground, surface and the whole industry) reached their lowest levels in 2001 (see Figure 12).

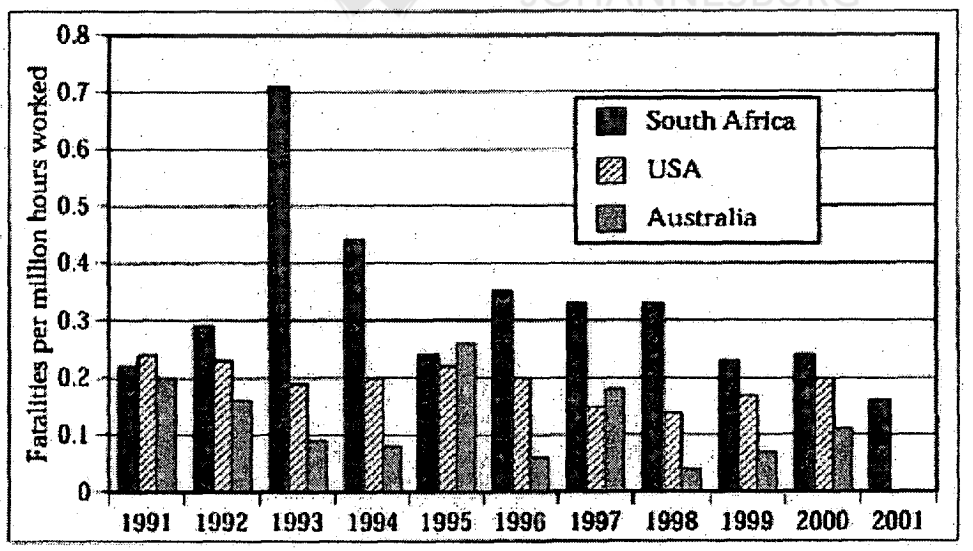

Figure 12. International comparison - fatality frequency rates on coal mines [32]

CHAPTER 4

4 Part 2: Metastable steels

4.1 Introduction

This chapter is part 2 of literature reviews on the type of material that was used previously for similar application. A metastable austenatic stainless steel selected to be used as a strain monitor-measuring device. This is due to the transformation characteristic of it.

4.2 Austenitic Stainless Steel

Stainless steel development, application and research thereof, have been significant for more than 50 years[33]. During this time, stainless steels have been used in many applications where material requirements demand extreme versatility, e.g. rustproof, tough, weldable and strong. Their stainless nature ensures low maintenance costs.

Austenitic stainless steels are, by far, the most popular grades and derive their name from the dominant phase present at room temperature, i.e. austenite, which is sometime called γ (gamma) phase. This particular phase has a face-centred cubic (FCC) crystal structure and is non-magnetic (more correctly paramagnetic); the structure ensures excellent toughness and ductility.

The use of austenitic stainless steels is complicated by the metastability (unstable) of the austenitic structure of most alloys. Their metastability leads to a martensitic transformation (usually non–magnetic $\rightarrow$ magnetic but not always); also a volume change is experienced. These effects may have a significant design consideration in applications requiring close dimensional tolerances or the absence of a ferromagnetic phase.

Upon cooling[1] (athermal martensite), under applied elastic stresses (stress induced martensite), or during plastic deformation (strain–induced martensite or SIM), the austenite phase (γ) of Fe–Cr–Ni (or Fe–Cr–Mn) may transform to body–centred tetragonal martensite (α') and/or hexagonal–close–packed (hcp), (ε) martensite phase.

The actual alloy chemistry affects the chemical free energy difference between the two phases. It should be noted that 65–70% of the world consumption of stainless is Type 304 which is a metastable alloy (18Cr–8/9 Ni). Type 310 (AISI 300 series) contains 25% Cr and 20% Ni and is stable with respect to martensitic transformation.

4.2.1 Empirical Models of Composition-Property Correlation

The contribution of elements to the particular properties of stainless steels is a well-explored field, and has led to a number of simple empirical models for various properties[34]. These models provide a basis for the comparison of elements based on their ability to form and stabilise austenite, decompose to intermetallic compounds or martensite, and their contribution to pitting corrosion resistance, among others. A formulae that relates tensile strength and yield strength to composition for stainless steels is given below:

Tensile Strength (MPa) = $470 + 600\cdot(N + 0.02) + 14\cdot Mo + 1.5\,\delta + 8\cdot d^{-0.5}$ (1)

Yield Strength (MPa) = $120 + 210\cdot\sqrt{(N + 0.02)} + 2\cdot Cr + 2\cdot Mn + 14\cdot Mo + 10\cdot Cu + \delta\cdot(6.15 - 0.054\cdot\delta) + (7 + 35\cdot(N + 0.02))\cdot d^{-0.5}$ (2)

where d is the grain size (in mm) and δ is the delta ferrite content (in vol. %).

4.2.2 Austenite Transformation to Martensite

The M_s temperature can be applied practically in alloy design, since it determines at what temperature the alloy can be used. The M_s temperature can be calculated with a fair degree of accuracy using the composition of the alloy, provided a suitable equation is used. Equation 3 was developed by Hull[35] using his Ni_{eq} (equation 4), and so is suitable for application to stainless steels.

$$M_s = 1482 - 47\times Cr - 59\times Ni - 54\times Mn - 37\times Si - 56\times Mo - 180\times Ti - 2390\times C - 3720\times N \quad (3)$$

where M_s = martensite start temperature (°C)

X = element concentration (wt%)

$$Ni_{eq} = Ni + 0.41\times Co + 0.11\times Mn - 0.0086Mn^2 + 0.44\times Cu + 24.5\times C + 18.4\times N \quad (4)$$

where X = element concentration (wt%)

A similar approach is used to determine the effect of elements on the stability of austenite during deformation. There is a relation between the degree of deformation, the temperature at which deformation occurred and the amount of martensite formed, but past work has generally kept the degree of deformation fixed and varied the temperature of deformation.

The temperature is the M_{d30} temperature, and can only be used to illustrate the effect of the composition on the tendency to form martensite during deformation. Equation 5 was developed by Angel[36]. The M_{d30} is for the presence of 50% martensite after 30% deformation or the temperature at which 50% martensite is produced under the action of a true strain of 0.30

$$M_{d30} = 413 - 14\times Cr - 9.5\times Ni - 8.1\times Mn - 9.2\times Si - 18.5\times Mo - 462\times C - 462\times N \quad (5)$$

where M_{d30} = temperature (°C) at which 50% martensite is produced by 30% deformation

X = element concentration (wt%)

4.2.3 Concept of an Md Temperature

The transformation from austenite to martensite occurs over a temperature range, the upper temperature of which is referred to as Ms (s=start), and the lower temperature of which is referred to as the Mf (f=finish). These temperatures depend on the composition of the steel and an austenitic grade of stainless steel can be considered to be steel in which the temperature at which the transformation from austenitic to martensite starts (Ms) is below room temperature. Where the Ms temperature is above room temperature, the steel will be partially or fully martensitic.

Of more interest to this work is where the martensitic transformation may be induced by deformation of the material at temperature above the Ms temperature (in particular at ambient temperature or above). The upper temperature at which transformation to martensite may be induced by deformation is given as Md (d=deformation) temperature. Again, this temperature is dependent on the chemistry of the alloy.

Empirical equations[36,37,38], relating the stability of austenite during deformation (M_{d30}) have been developed and are summarised in Table 1.

Table 1. Alloying element coefficient for calculating M_{d30} temperatures[36, 37, 38]

Equivalent Coefficient (°C/wt%)			
Element	**Angel[36]**	**Pickering[37]**	**Nohara[38]**
Base	413	497	551
C	-462	-462	-462
N	-462	-462	-462
Mn	-8.1	-8.1	-8.1
Ni	-9.5	-20	-29
Cu	-	-	-29.0
Cr	-13.7	-13.7	-13.7
Mo	-18.5	-18.5	-18.5
Si	-9.2	-9.2	-9.2

These equations are an attempt to calculate the Md_{30} temperature. The effect of the alloying elements is assumed to be additive and to vary linearly with the percentage of elements by weight[36]. The relevance of Md_{30} to a practical situation needs to be kept in mind. A major difference between these formulae is the base coefficient and this reflects the range of compositions studied; residual elements may also effect the determination of Md_{30}. Various experimental techniques involving magnetic testing, metallography, tensile testing, dilatometry, electrical resistance can be utilised to determine Md.

Figure 13 shows the variation obtained in Md_{30} for AISI 304 stainless steel showing the effect of chemical composition change[39]. The calculation is based on using Angel's formula.

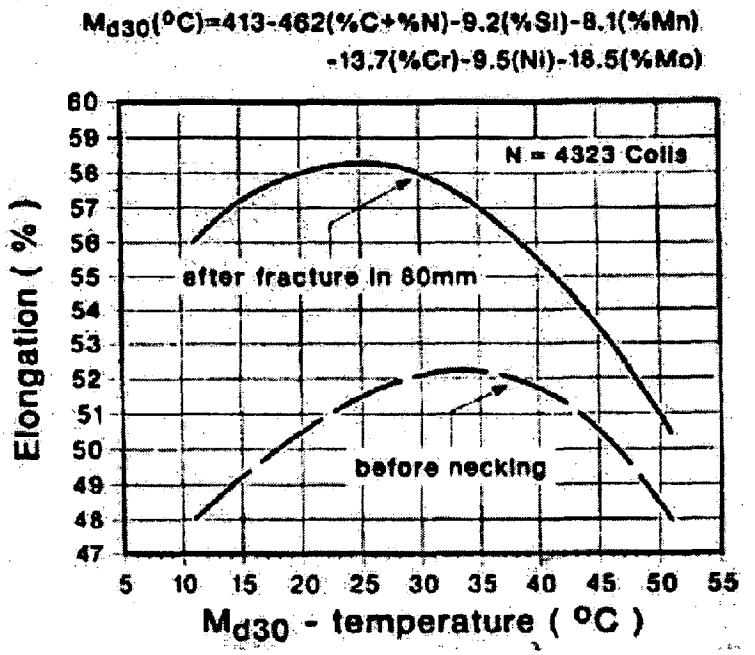

Figure 13. Range of M_{d30} calculated for AISI 304 stainless steel and its influence on ductility [39]

4.2.4 Stress –Strain characteristic

In a metastable austenitic stainless steel, (polycrystalline alloy) where α′ martensite can be induced by deformation, three distinct stages are present in the stress–strain curves, as shown in Figure 14. For a large number of alloys, the rate of work hardening increases and then becomes constant over a relatively large amount of plastic deformation. The volume percentage of α′ martensite is linearly related to plastic deformation in stageIII.

The instability of each particular alloy will determine the size of stages I and II, with unstable compositions showing a reduced stage II, which is commonly called the "easy glide" range. ε (Epsilon) martensite formed during stages I and II transforms to α′ (alpha prime) martensite in stage III.

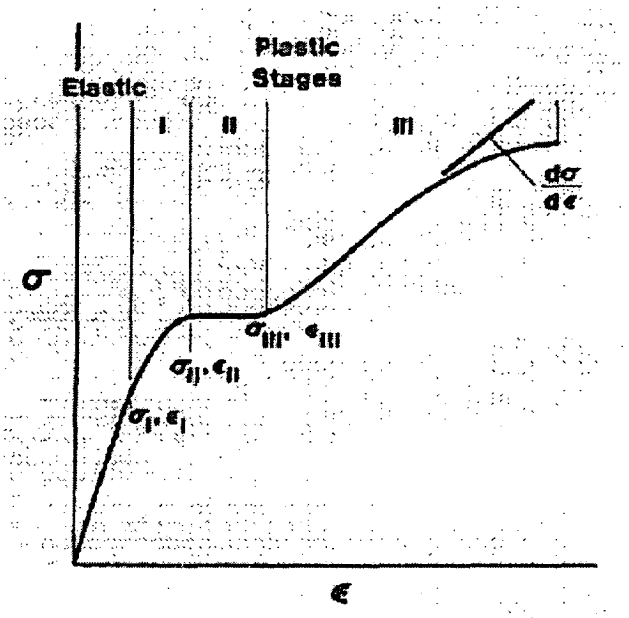

Figure 14. Three stages of work hardening for metastable austenitic alloys[40]

Stress-strain curves for three commercially available austenitic grades with superimposed martensite content (α') are shown in Figure 15 (Type 301–Cr and Ni lowered to increase work hardening, Type 304L– carbon reduced to improve weldability, Type 201–N and Mn partly replace nickel). Types 201 and 304L stainless steel show high strains to failure but the martensite (α′) occurs more slowly and at higher strains than in Type 301. The latter grade displays a sigmoidal stress–strain curve. Inflexion points in the curve for Type 301 are associated with the beginning and end of the strain–induced $\gamma \rightarrow \alpha'$ transformation. It is also noticeable that a few percent plastic strain is necessary to produce α′ martensite in Type 301. Comparison can be made between Figure 14 and Figure 15 with regard to this particular alloy.

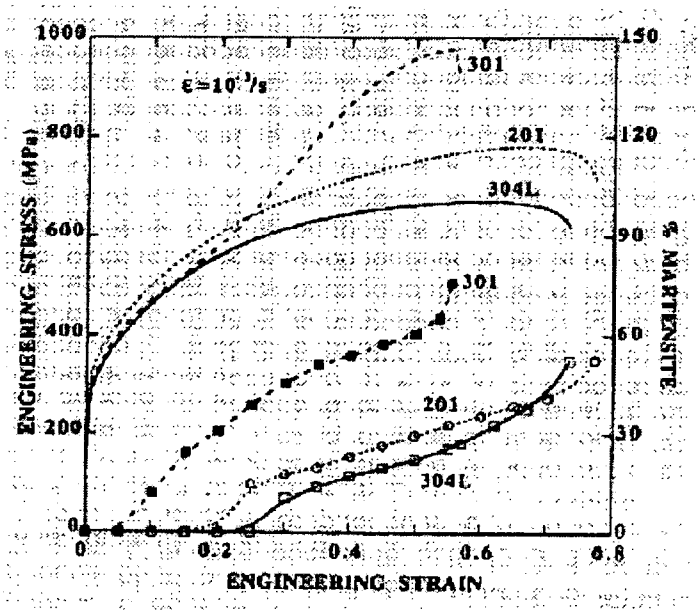

Figure 15. Stress –strain characteristics and α′ martensite for alloys 201, 301 and 304L at room temperature[41]

Hecker[42] used a magnometer and saturation magnetization measurements to calibrate 'Ferritescope' readings. A calibration curve can then be constructed to convert 'Ferritescope' readings (Figure 16), into volume fraction martensite transformed. An alternative is to calibrate against X–ray measurements.

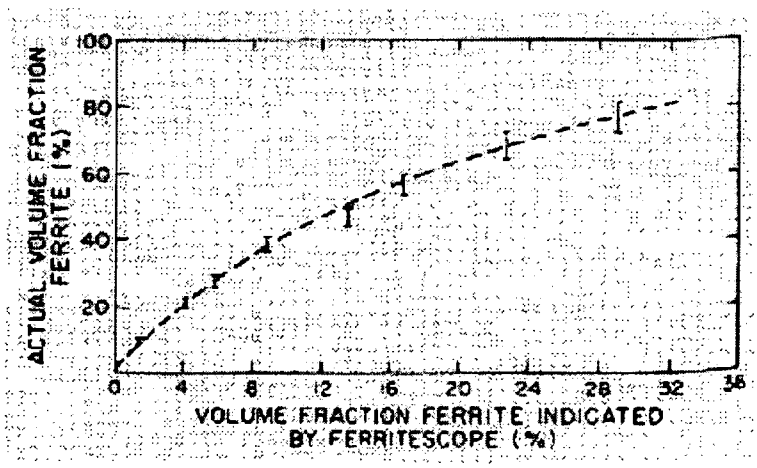

Figure 16. Calibration curve of actual % martensite versus that indicated using a "ferritescope" (every alloy requires its own curve)[42]

4.3 TRIP Steels

TRIP is the acronym for Transformation Induced Plasticity. The name already indicates that obviously plasticity can be affected by phase transformation. The name TRIP, however, has been used for a much wider field of phenomena related to phase transformation and the overall deformation behaviour of a specimen. A TRIP steel was first "discovered" in the United States at the University of Califonia at Berkeley, while an investigation into tougher structural steels was in progress[43]. Although it has been known since the 1960's that TRIP steels have, in general, superior toughness and strength properties it is only recently that the "smartness" of the material has been realised.

Doege and Kulp[44] investigated the forming behaviour and properties of two types of TRIP steels, low alloyed (L-TRIP) and high alloyed (H-TRIP). In their work two different steel composition were examined. The chemical composition of both L-TRIP (TRIP700) and H-TRIP (Type 304SS) steels is given in Table 2. The H-TRIP belongs to the group of stainless steel materials, whereas the L-TRIP is not.

Table 2. Chemical composition of the TRIP steels used[44]

	C	Mn	Si	P	S	Cr	Mo	Ni	N
TRIP700	0.106	1.42	1.5	0.004	-	-	-	-	-
AISI 304	0.06	0.82	0.3	0.010	0.007	18.31	0.02	8.28	0.0183

For the examination of mechanical properties, uniaxial tensile test was performed and the results are shown in Table 3. L-TRIP material TRIP700 and the H-TRIP materials AISI304 indicate different forming characteristics. The work hardening exponent n and the uniform elongation A_g as well as the elongation at fracture A_{80} of the high alloyed TRIP material is at least twice as high as for the low alloyed TRIP steel.

TRIP-steels contain austenite, which is metastable at room temperature. It transforms to martensite during straining (TRIP effect). During the transformation the metastable austenite transform to martensite which increases the resistance to local necking. This process improves the product of strength times ductility balance of these steels (σ_{UTS} X ε_f). The ductility of L and H TRIP steels is higher; and their strength is lower.

Table 3. Mechanical properties of the analysed materials[44]

Material	S_o mm	RD	A_g %	A_{80} %	YS MPa	UTS MPa
L TRIP TRIP700	1.50	0	25	31	436	719
		45	24	28	441	719
		90	23	27	453	726
H TRIP AISI304	1.00	0	44	48	316	625
		45	47	52	296	581
		90	48	53	293	582

Where: **RD** is the rolling direction, A_g is uniform elongation and A_{80} is the percentage elongation at fracture

For the last 20 years, the steel industry introduced new steel categories such as high strength low alloy steels (HSLA), the interstitial free high strength steels (IF-HS), and the dual phase steels (DP-steels)[45]. However, for the past 10 years TRIP steels have been investigated and as can be seen from Figure 17, their mechanical properties are somewhat different from all the previous steel grades. TRIP steels can offer a much better combination of strength and ductility.

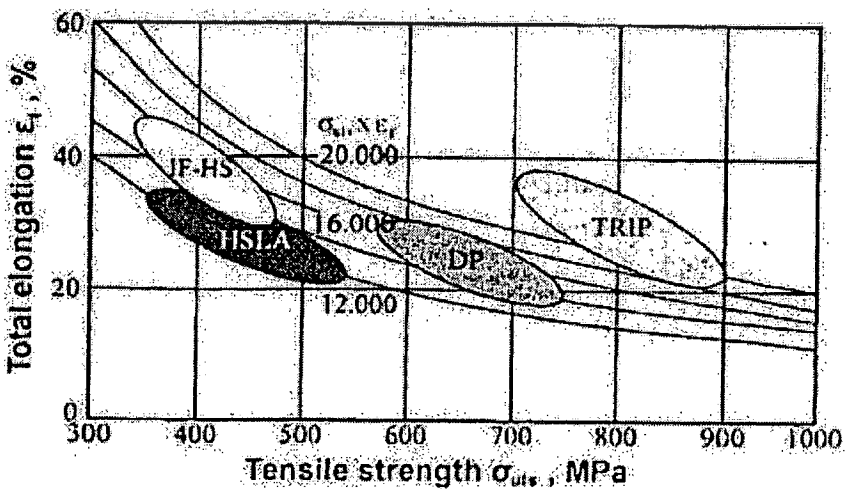

Figure 17. Comparison of different steel grades in terms of strength and ductility combination[44]

4.4 Requirements for a Sensor Material to be used in Mining Environments

TRIP (Transformation-Induced-Plasticity) steels are materials, which change state from austenitic, non-magnetic to a martensitic, ferromagnetic phase as the material undergoes straining[45]. There is direct correspondence of the peak strain level experienced in the material with the percentage of ferromagnetism, hence monitoring the relative amount of the ferromagnetic content will indicate the level of strain (and therefore stress). The phase transition that accompanies the straining is irreversible so the gauges retain the peak strain until that value is subsequently exceeded.

The TRIP steels may undergo transformation during the early or later stages of macro strain behaviour. For an alloy to be used as a strain monitor it must fulfil the following requirements:

- Yield strength similar to existing carbon steel rockbolts
- Ability to withstand conditions of high tensile and shear stress
- Resistant to corrosion in the mining industry
- Low incubation strain for transformation plus substantial transformation rate without strain
- Ease of manufacturing and monitoring using a simple (conventional) technique

CHAPTER 5

5 Experimental Technique

5.1 Introduction

This chapter outlines the experimental technique followed in the development, processing, and laboratory characterisation of the smartbolt material. Also, selections of testing site, an installation and monitoring of prototype rockbolts.

Prior to conducting the experimental program, a series of preliminary tests was performed to determine the experimental set-up, including modelling of material, boundary conditions, holding frames, specimen sizes, loading rates and design of bolts, as well as how to minimise any induced bending or stress. The concept and the set-up of the experiments are presented in the following sections.

5.2 Material production

Two octagonal one ton ingots of smartbolt material were successfully rotary forged down to a section size of 140 mm square at Ispat Iscor Long Steel Products. This was finally rolled through the 12-stand bar mill to wire rod (20 mm in diameter). The chemical composition and nominal specification of the smartbolt alloy is given in Table 4. The nominal specification was chosen from the range of composition studies.

Table 4. Nominal and analysed composition of the Smartbolt alloy (wt%)

	Elements (wt%)								
	C	**Si**	**Mn**	**P**	**S**	**Cr**	**N**	**Mo**	**Cu**
Nominal	0.2* min	-	8 to 12+	0.025 max	0.025 max	11 to 13#	0.1 max	-	-
Analysed (spectroscopy)	0.233	0.61	9.99	0.014	0.0091	12.5	0.13	0.02	0.07

** preferably 0.25 ±0.02, + preferably 10 ±1.0, # preferably 11.5 to 12.5*

5.3 Laboratory characterisation

5.3.1 Test Specimens

A laboratory study of the influence of uniaxial stress, multiaxial stresses and strain on the industrial annealed smartbolt material was conducted. To study the transformation characteristics and determine the mechanical properties, tensile tests were carried out on two sets of round specimen (6.25 and 12.5mm diameter gauge length). Also, a correlation of the tensile test results with ultrasonic sound velocity was performed.

A series of 20mm diameter mini bolts (approximately 750 mm and 400 mm in length) as shown in Figure 18 were tested and the load, strain, % ferromagnetism (indicated by a ferritescope), and longitudinal sound velocity values were recorded.

Metallography was carried out by way of automated grinding and polishing. Laboratory and industrial annealed specimens were mechanically polished to a 1μm finish using diamond paste, and finally electropolished in 20 percent perchloric acid at 18 volts for 30 seconds (20ml perchloric acid plus 80ml alcohol) followed by electroetching in 10% oxalic acid reagent. Electrochemical polishing was necessary to remove any deformation-induced martensite that may have formed during the mechanical preparation.

5.3.2 Testing Apparatus

A computer interfaced Instron 1175 tensile machine (which allows the tensile data to be captured on a computer file) was used to conduct interrupted tensile tests (a modification of testing to ASTM E8[46]). The Tinius Olsen Super L system 600kN frame shown in Figure 18 was also used for tension testing of mini bolts. Laboratory simulation was carried out whereby multiaxial loading (compression test) was simulated by cold rolling in a 2-high laboratory rolling mill shown in Figure 19. The influence of strain on transformation was measured using magnetic and ultrasonic methods.

Ultrasonic velocity is a physical property influenced by microstructural features. A change in microstructure by the use of applied stress may be potentially monitored by accurately measuring longitudinal ultrasonic velocity. For this project an ultrasonic sound velocity-measuring device was used. This is an expensive but accurate measuring device.

A Krautkramer USM 25 DAC ultrasonic measuring instrument was used to measure the sound velocity of the mini-bolts at different strain levels. Also a ferritescope, shown Figure 19 was used to measure the amount of martensite (ferrite) transformation. Calibration of the instrument was performed according to ASTM E494-75[47] and the Krautkramer operating manual[48]. It should be noted that Type 304 stainless steel was taken as a reference material.

Testing procedure for uniaxial tension was as follows:

a) switch on the main power via the key-switch on the hydraulic power-pack

b) put the auto/manual switch to manual and press slow

c) using the correct wedge action grips (v-grips) for round specimens, insert a mini bolt on the test frame and tighten it

d) select the required measurement units

e) zero the load on the control panel

f) test at a slow speed to the required load and stop the test

g) use a Ferritescope meter to measure the % transformation or ferromagnetism at that load

h) also, use the ultrasonic measuring instrument to measure the sound velocity of the mini-bolts at that load

i) repeat step c to h on different mini-bolts (up to 200kN load).

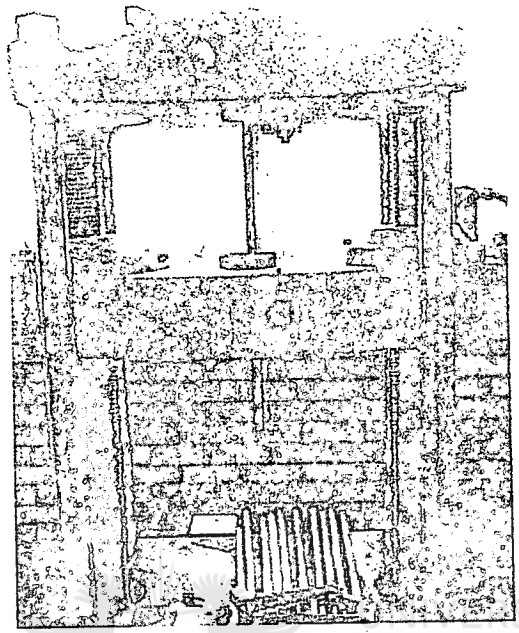

Figure 18. The Tinius Olsen Super L system 600kN frame tensile machine

Testing procedure for compression or multiaxial studies was as follows:

a) soak the mini-bolt in a furnace at 1200°C for an hour

b) slightly forge it to get a flat surface (i.e. from 20mm to 18mm)

c) anneal at 1050°C for 30 minutes and water quench

d) grind the top and bottom flat section of the mini-bolt

e) measure the % transformation or ferromagnetism on flat section using a Ferritescope

f) also, measure the length, thickness, width and sound velocity prior to rolling

g) deform the specimen to the required thickness (% reduction in area)

h) repeat steps d to g until the required % reduction in area has been reached

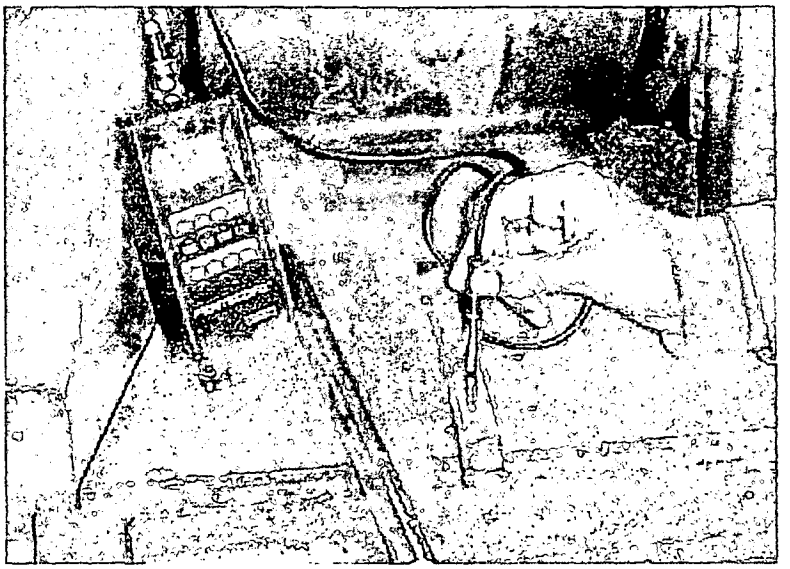

Figure 19. Two-high laboratory rolling mill, smartbolt bars and a ferritescope

Tension and compression data were recorded. From this data, it was possible to construct a calibration curve of velocity versus stress and strain. Also, modelling of uniaxial and multiaxial stress was enabled.

5.3.3 Parameters Calculated

The following parameters were calculated:

Elongation (e) :

$$e = \frac{l_1 - l_0}{l_0} \cdot 100 \qquad (6)$$

where e = elongation (%)

l_o, l_1 = initial and final specimen gauge lengths

Reduction in area (r):

$$r = \frac{t_o \cdot w_o - t_1 \cdot w_1}{t_o \cdot w_o} \cdot 100 \qquad (7)$$

where r = reduction in area (%)

t_o, t_1 = initial and final specimen gauge thickness

w_o, w_1 = initial and final specimen width

5.3.4 Modelling of smartbolt material

Some preliminary modelling work in uniaxial loading condition was carried out to assess the plastic behaviour of these metastable austenitic stainless steels of which the smartbolt alloy is part. Microsoft's Excel SOLVER package was used as the computational tool to analyse the load-strain data.

Loading underground is not necessarily uniaxial but a mixture of tensile, shear and frictional forces. Therefore a preliminary laboratory simulation (modelling in multiaxial loading) was carried out whereby multiaxial loading was simulated by cold rolling in a 2-high laboratory mill. The influence of strain on transformation was measured with a magnetic method (ferritescope).

All data fitting was performed using Excel. Two methods were used for optimising the fit:

- standard polynomial regression curves were used to determine empirical relationships
- non-polynomial relationships were optimised numerically using the "Solver" routine in Excel

5.4 Selection of testing site

South Deep Gold mine was chosen because it is known that the gold mines are deeper than platinum ones and the rock morphology (reef ore) is unstable due to its weak tensile properties. Also, rockfalls commonly occur at gold mines.

5.4.1 History

Initial production at South Deep gold mine started in 1968, owned by Western Areas Limited. The size of the mining authorisation area extends over 3,563 hectares of mineral rights. Placer Dome obtained a 50% share of the Western Areas Limited mine in April 1999.

5.4.2 Shafts

South Shaft has six compartments (surface to 50 level and depth below collar is 1303m). The depth of these compartments (SV1, SV2 and SV3) are 1935m, 2785m and 2785m below the surface, respectively. SV3 was chosen to be the testing site for the Smartbolt™ technology because of its depth and geology.

5.4.3 Mining Methods

Two main mining methods are currently used at South Deep. Half the gold produced originates from narrow conventional mining (mini-long wall, with backfill). Hand held drills and rail bound equipment is used. Trackless mechanized drift and fill mining will produce the other 50% of gold. Low profile front-end loader and rubber tyre service equipment are used as well as hydraulic drill rigs.

5.4.4 Geology

To the west of the sub-crop we have the Ventersdorp Contact Reef (VCR), and to the east we have the massive Elsburg reefs consisting of the MB reef, the MI reef, the MA reef, the EC reef. Average ore body dip is 18° to the South. Reef ore is unstable due to its weak tensile properties.

5.5 Installation technique

It was found that the proposed test site used 20mm diameter by 2400mm long roofbolts. The threads (M20 RH) of the bolts were machined according to SABS 1408 of 1987 (code 142037). The thread length was approximately 150mm in length. One hundred smartbolts were prepared, however, for this project only thirty-four smartbolts were installed.

The Smartbolts were not thread rolled but machine threaded, because the material has a much stronger work-hardening effect (in order to thread roll the material a special set of dies with high hardness is required). One set of fourteen smartbolts (2.4m x 20mm) were installed in shaft 1, level 94 west, number 2 haulage tunnel and the other set of twenty at level 94 haulage ramp.

All sets of Smartbolts were cement bonded and mechanically anchored so that when the rocks get loose during blasting, the cement can hold the bolts (it is felt that the smartbolt technology may be more appropriate using anchoring rather than frictional forces).

The Smartbolts were installed as follows:

Step 1	position temporary supports according to the mine standards
Step 2	drill hole 5cm shorter than total bolt length (or the length of the steel minus the thickness of the nut plus the washer)
Step 3	remove plastic cover from the 35mm-expansion shell, twist shells slightly by hand so that it just begins to expand

Step 4	place the bolt in the hole
Step 5	place the M20 nut on the bolt
Step 6	rotate bolt slowly to expand anchor
Step 7	when resistance increases, continue until the bolt is stiff or tight
Step 8	mix cement and place it in a grouting machine
Step 9	connect a breather pipe to the grouting machine and insert it into the hole parallel to the bolt
Step 10	pump in the grouting cement until the hole is full
Step 11	place a washer and nut on the bolt and use a torque wrench to torque the bolt up to 30Nm
Step 12	continue the rotation until torque wrench stalls (reaches a set value) or washer visibly bites into roof

Steps 2, 8 and 12 of the installation process for a rockbolt is also illustrated in Figures 20, 21 and 22 respectively. These show the drilling stage prior to installation of the required roofbolt, mixing of the cement in a grouting machine, and tensioning or tightening of a roofbolt to an appropriate load using a torque wrench.

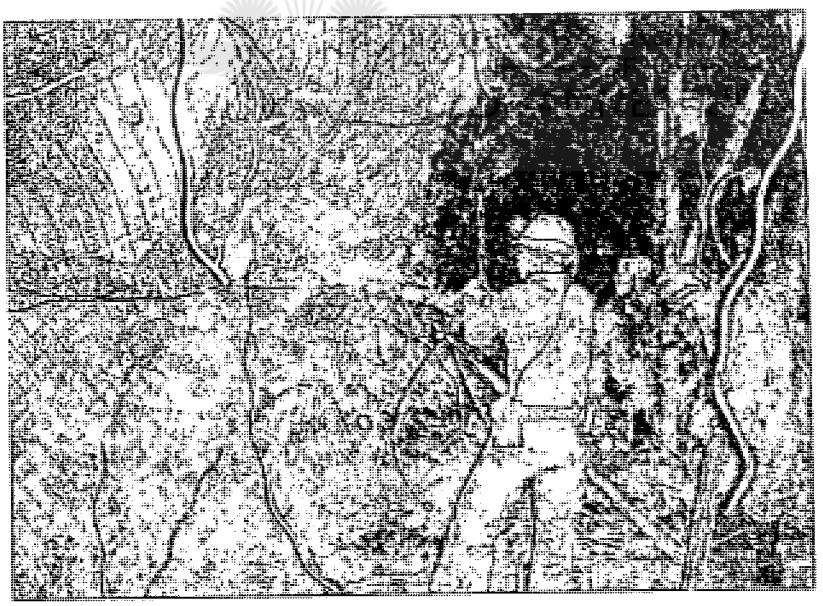

Figure 20. The drilling stage prior to installation of the required roofbolt at a South African gold mine test site

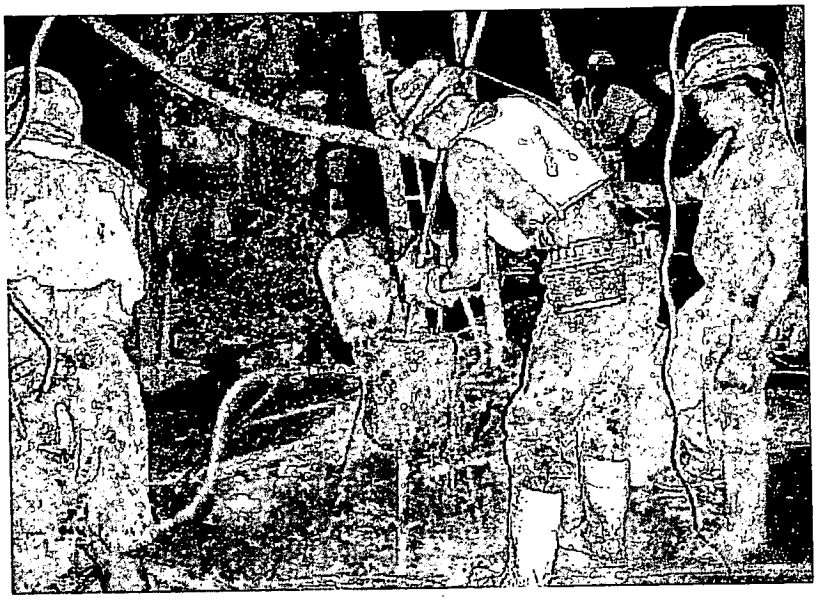

Figure 21. Cement mixing in a grouting machine

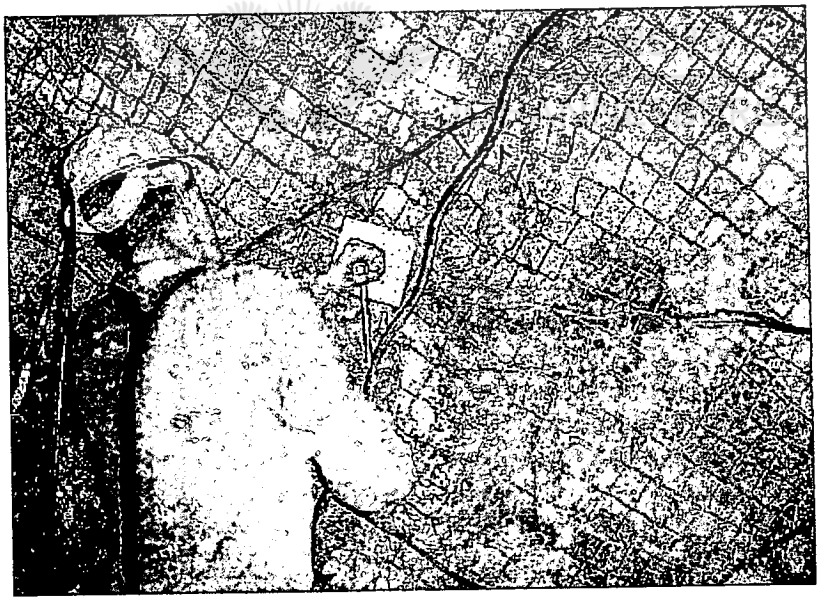

Figure 22. Tensioning of the roofbolt after installation

For mechanically anchored installations, the maximum torque setting on the roofbolter is usually 150 Nm, or such that the load transferred to the bolt is 50kN. This should be tested in the workshop by tensioning a bolt with a hydraulic jack. The figures quoted with regard to torque settings correspond to industry usage. This is in fact a complex matter, one that has perhaps not received the attention it deserves. The important parameter in tensioning the bolt is the tension transferred to the bolt as a result of the torque.

There is no single relationship between the applied torque and the resultant tension, it being the bolt diameter, the pitch of the thread on the bolt, the friction between the nut and the washer, etc. Mechanical anchors are sometimes acceptable, especially in hard sandstone where it is difficult to drill holes thinner than 32mm diameter. The disadvantages are that in the absence of grout filling, they are susceptible to corrosion. Anchors may creep since the anchor resistance is fixed at 50 or 100 kN. What is not commonly appreciated is that once the bolt relaxes (due to for instance frittering of the roof underneath the washer), the anchor itself may lose grip due to relaxation.

In cases where mechanical anchors are used, the bolt diameter only needs to be thick enough to be 1.5 times stronger than the required anchor resistance. The major disadvantages of resin point anchors as compared to mechanical anchors is that the installation procedure is more complex, requires more discipline, and that seasonal fluctuations in temperature may require adjustments to the installation procedure. It is also often necessary to use a thicker bolt than would be required from a strength point of view, merely to ensure proper mixing of the resin.

5.6 Monitoring

The pre-installation monitoring was done in three phases: prior to delivery to the mine, after delivery, but prior to despatch underground on the mine, and finally after dispatch underground, but prior to installation in the section. Monitoring is the final step in the roofbolting process. It is a continuous processes not an act, as much part of the bolting exercise as drilling a hole into which to install a bolt. It should consist of monitoring the bolts prior to installation and after installation. The threads on the bolts and nuts should be checked for damage by the roofbolter crew prior loading the bolts on the bolter.

There are a number of devices available with which roof deflection can be measured to supply prior warning of roof falls (as discussed in section 2.4). For this project an ultrasonic sound velocity-measuring device was used. The instrument used in this work is expensive but accurate measuring device. As indicated earlier, a Smartbolt^{TM} undergoes crystallographic transformation under stress, therefore the device measures this change.

Monitoring of the loading on the bolts was initially carried out on a weekly basis in order to collect all the information. The load is distributed to the surrounding rock by means of the base plate/washer. The ultrasonic velocity of the bolt after installation is then measured using the ultrasonic instrument. The results are then superimposed on a calibration curve to obtain the amount of stress and strain the Smartbolt™ and the surrounding rock experiences.

CHAPTER 6

6 Results and Discussion

6.1 Introduction

This chapter outlines the results and a discussion of all the work performed including modelling of Smartbolt^{TM} alloy under uniaxial and multiaxial loading conditions, construction of calibration curve and underground testing of the Smartbolt^{TM} material.

The results obtained in this project are categorised into laboratory characterisation, uniaxial and multiaxial modelling of the material, and testing of prototype rockbolts on the mine. Rockbolts function as reinforcement to increase the shear strength or bearing capacity of the rock mass by providing confining stress as well as tensile and shear resistance to the rock mass and the rock joint. However, the Smartbolt^{TM} functions as a strain monitor as well; it measures the amount of multiaxial stress in the rock mass.

6.2 Microstructures of Smartbolt^{TM} alloy in annealed and strained conditions

The laboratory and industrial annealed microstructures of Smartbolt^{TM} alloy were similar (fully austenitic) with no presence of carbides. Figure 23 shows the electrolytically polished and etched Smartbolt^{TM} alloy that consists of austenite grains with twinning. The black spots seen in this micrograph are non-metallic oxide inclusions. Martensite was not detected in the alloy in the annealed state because of the low M_s temperature (temperature at which martensite start to form). The martensite can often be induced above the M_s by cold work and this occurs up to a temperature that is designated as M_d (highest temperature where plastic deformation can still induce martensite nucleation) where $M_d > M_s$. A micrograph of a lightly strained Smartbolt^{TM} alloy is shown in Figure 24 and consists of bands of finer twinned martensite (strain induced martensite) in an austenite matrix. The formation of martensite plates is assisted by a positive elastic tensile stress, the shear and normal strains. It is clear that the Smartbolt alloy undergoes transformation during the early stages of straining.

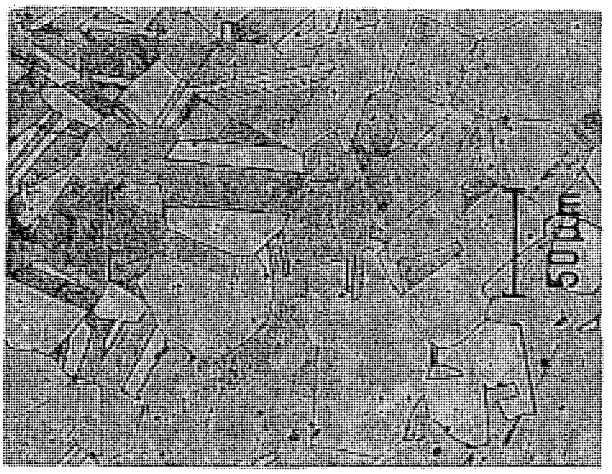

Figure 23. Optical micrograph of Smartbolt™ alloy in annealed condition

Figure 24. Optical micrograph of strain induced martensite in a Smartbolt™ alloy

6.3 Characterisation of Smartbolt™ alloy under uniaxial loading conditions

Transformation characteristics under uniaxial tensile testing were studied, and, Figure 25 shows the amount of martensite (measured as % magnetism) formed during tensile testing as a function of percent elongation. This study was carried out to determine if this material could be used as a strain-monitoring device. The martensite (α') (see Figure 24) obtained from plastically deformed austenite (γ) is ferromagnetic and is readily detected by magnetic measurements. The magnetic permeability of a sample was measured with a ferritescope. This is a two-point probe which, when placed on a sample is energised by the low frequency magnetic field and induces a voltage. This voltage induced is a direct measure of the magnetic permeability.

The tensile properties for the alloys tested at room temperature are summarised in Tables Table 5 and Table 6. The annealed proof values are fairly similar to the current carbon steel grade used for roofbolts. The proof stress of the smartbolt alloy in the hot rolled and annealed (HRA) condition is 438 to 451MPa, which is somewhat higher than that for Type 304 (319MPa).

The UTS of the smartbolt alloy in the HRA condition was 961 to 1039MPa for the laboratory and industrial annealed material, respectively. The UTS values, relative to the proof stress values, are an indication of the instability of the alloy. It is clear that the smartbolt alloy is the most unstable alloy, and has a relatively high ratio of UTS/Proof. Typical values for the tensile strength of industrial Type 304 are 560 to 635MPa.

The minimum elongation specified for Type 304 is 40%, compared to that of the smartbolt alloy, which is 25 to 30%. Bressanelli[49] proposed that because of the limited ductility of the martensite phase, premature fracture might occur that results in decreased uniaxial ductility. In the smartbolt material, alpha prime (α') martensite is nucleated very quickly and hence this will reduce the % elongation and produce a characteristic flat-face fracture.

Table 5. Tensile tests results (12.5mm diameter specimens)

Alloy	UTS (MPa)	0.2%Proof Strength (MPa)	Elongation (%)	Condition
Smartbolt™	1039 ±41	445 ±21	29	Lab annealed
Smartbolt™	961 ±9.0	451 ±39	25	Industrial annealed

Table 6. Tensile tests results (6.25mm diameter specimens)

Alloy	UTS (MPa)	0.2%Proof Strength (MPa)	Elongation (%)	Condition
Type 304	733 ±1.0	319 ±63	83	Lab annealed
Smartbolt™	1063 ±24	438 ±2.0	30	Lab annealed

It is clear that the smartbolt alloy undergoes transformation during the early stages of plastic behaviour (with low incubation period, $e_{sm} \approx 2$) unlike the commercial Type 304 which has a higher incubation period ($e_{304} > 15$) and requires at least 16% plastic strain to give a measurable response. In the smartbolt material, α' martensite is nucleated quickly and hence large amount of α' martensite will reduce the % elongation, as, shown in Figure 26 (a blow-up bottom section). It can be seen that the incubation strain of the smartbolt alloy is reduced (≈2%) and that the microstructural transformation rate is high, thus enabling effective monitoring.

The product of high yield strength and uniform ductility of a Smartbolt™ alloy is slightly higher than that of TRIP steels. By extrapolating Figure 17, it can be seen that the Smartbolt™ alloy lies to the right hand side of the TRIP grades, which have a σ_{UTS} X ε_f of about 2x 10^4 MPa. Therefore, this material offers a better combination of strength and ductility.

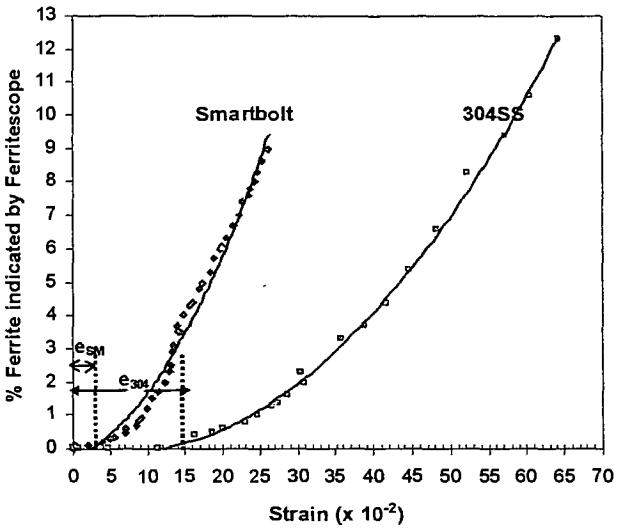

Figure 25. Percentage ferromagnetic phase versus strain for Smartbolt™ alloy and Type 304 stainless steel as determined by a ferritescope

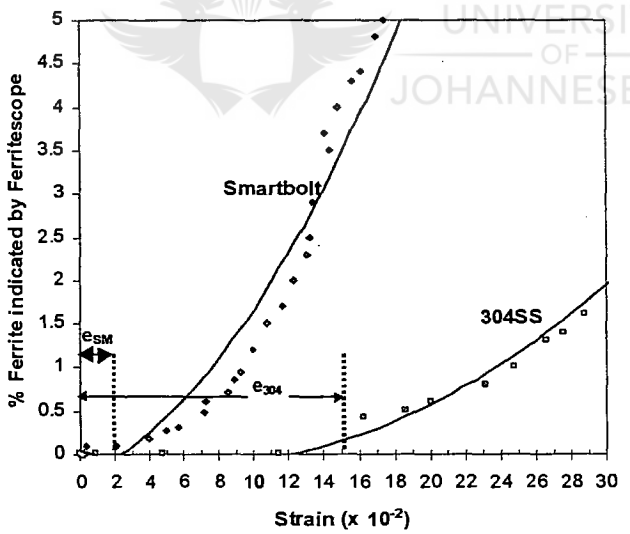

Figure 26. Percentage ferromagnetic phase versus strain for Smartbolt™ alloy and Type 304 stainless steel showing a clear incubation period

6.3.1 Modelling of Smartbolt™ alloy during uniaxial testing

This part of the work was undertaken to derive and verify a model for the plastic behaviour of the smart alloy together with a standard Type 304 stainless steel, both alloys being metastable with regard to the austenitic structure. The differences between a so-called 'smart' material and other materials can thus be quantified. In this work, only stress and strain in the uniaxial state was modelled. The objective was to determine the transformation constants of these alloys shown in a flow curve (equation 9), proposed by Ludwigson and Berger[50] and also to isolate their effects.

It has been found that the flow curve for many materials can be empirically described by the equation:

$$\sigma = K[\ln(1+e)]^n \qquad \text{.....} \qquad (8)$$

where σ = true stress, e = engineering strain, K = austenitic 'strength factor' (constant) and n = 'strain-hardening index' (constant).

Literature[50], however, reports that for some engineering materials like '18-8' stainless steel, the expression does not hold, and it is suggested that a strain-induced decomposition of austenite to martensite is responsible for this effect.

Ludwigson and Berger have therefore proposed an amended flow curve equation to incorporate both the true stress contribution of austenite at any level of strain and the true stress contribution of martensite at any level of strain:

$$\sigma = K[\ln(1+e)]^n\left[1-\left(1+\frac{e^{-B}}{A}\right)^{-1}\right]+C\left(1+\frac{e^{-B}}{A}\right)^{-Q} \qquad (9)$$

Where A = a constant representing the propensity of the material to transform to martensite, B = a constant to account for autocatalysis, C = martensitic 'strength factor' (constant) and Q = martensitic 'strengthening index' (constant).

The writers also showed that the volume fraction of martensite (*VFM*) could be related to the volume fraction of austenite (*VFA*) in metastable austenitic stainless steels by equation:

$$VFM = Ae^{B}(VFA) \qquad (10)$$

Since, the sum of *VFM* and *VFA* is unity, equation (10) can be rewritten as:

$$\frac{VFM}{(1-VFM)} = Ae^{B} \qquad (11)$$

and taking the logarithm of the expression above, thus yields:

$$\log\left[\frac{VFM}{(1-VFM)}\right] = \log A + B\log e \qquad (12)$$

A plot of log [*VFM*/(1-*VFM*)] versus log [*e*] therefore gives a straight line with slope equal to '*B*' and y-intercept equal to 'log *A*'. Using this relationship, the *A* and *B* values for the particular material can be determined Figure 27. The remaining four constants, *K*, n, *C* and *Q*, can then be determined by obtaining a best-fit approximation of the available experimental data.

From experiment, a range of data relating measured true stress, $\sigma_{measured}$, and engineering strain, *e*, is obtained. Equation (9) relates the unknown constants to a calculated true strain, $\sigma_{calculated}$.

The constants can then be calculated by minimising the sum of the square of the difference (i.e. error) between $\sigma_{measured}$ and $\sigma_{calculated}$. Microsoft's Excel SOLVER package was used as the computational tool.

The software relies on an initial best guess of the unknown constants, and through a series of non-linear regressions, modifies the values for *K*, n, *C* and *Q* such that over the entire range of experimental data, $\Sigma(\sigma_{measured} - \sigma_{calculated})$ is as small as possible.

In order to verify the results obtained, a plot of $\sigma_{measured}$ versus $\sigma_{calculated}$ can be made, and if sufficiently accurate numerical values for the unknown constants have been calculated, the plot should yield a straight line with slope equal to unity and a y-intercept equal to zero Figure 28. The constants measured for both steels are shown in Table 7 below.

Table 7. Flow-curve parameters for Smartbolt™ alloy and Type 304 stainless steel

Alloy	K (MPa)	n	C (MPa)	Q	A	B
Type 304	1200	0.35	1735	0.73	0.49	2.72
Smartbolt™	900	0.14	6690	1.04	1.98	2.16

The parameter C is the martensite analogue of the austenitic strength factor K. It can be seen that C is much higher in the Smartbolt™ alloy, reflecting the higher carbon content relative to Type 304. Conversely, K is somewhat higher in Type 304 due to its higher alloy content. The lower n value for the Smartbolt™ alloy reflects work hardening of martensite rather than austenite (see propensity to transform A value). The transformation response (A value) for the Smartbolt™ alloy is about four times higher than Type 304 stainless steel.

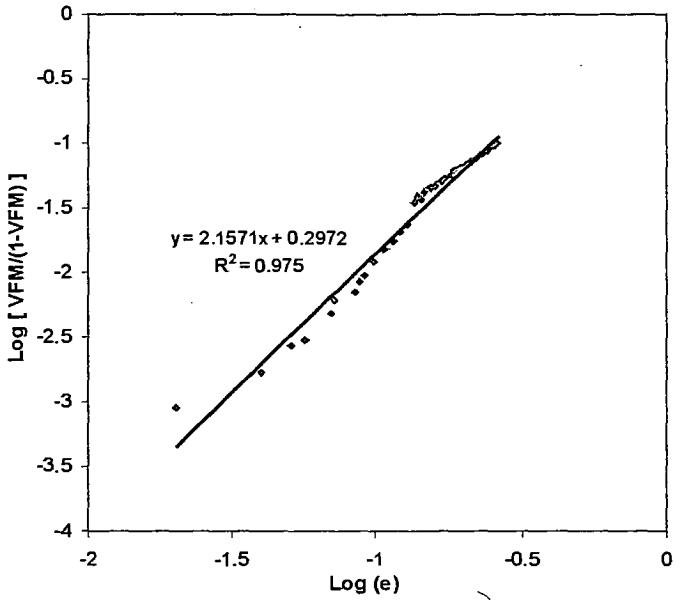

Figure 27. Verification of the transformation-deformation function for Smartbolt™ alloy

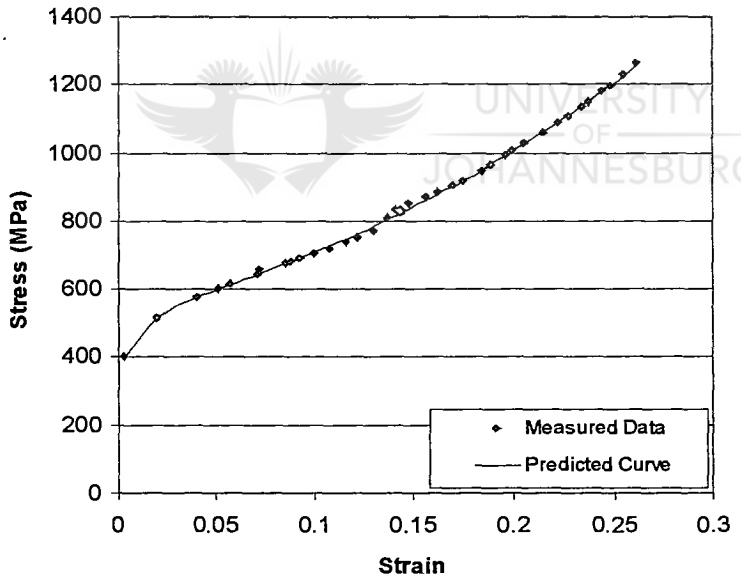

Figure 28. Measured and predicted stress as a function of strain for Smartbolt™ alloy

In this uniaxial modelling work a smartbolt alloy was compared with Type 304 stainless steel with regard to transformation characteristics. Based on mechanical properties and low incubation of smartbolt alloy, it might be used as a strain monitor. Type 304 stainless steel doesn't qualifies due to a high incubation strain and high cost (higher nickel content than the Smartbolt^{TM} alloy).

6.3.2 Influence of uniaxial strain on ultrasonic sound velocity

A calibration curve was constructed to determine a correlation between the stress, longitudinal ultrasonic velocity and strain. Also, to be able to draw-up some warning guidelines. Duplicate 750 mm long x 20mm diameter mini bolts were tensile tested and the load, strain, ferritescope, and longitudinal velocity values were recorded. A portable ultrasonic (USM 25 DAC) monitoring device was used to measure the longitudinal velocity during the calibration trials. The results of ultrasonic sound velocity measurements of the stressed 20mm diameter mini-bolts are shown in Table 8. They are also graphically illustrated in Figure 29. The results show a good correlation when using a linear relationship between the longitudinal ultrasonic velocity and strain with an R^2 value of 0.97. A plot of stress as a function of strain (Figure 28 in section 6.3.1) was then superimposed in Figure 29. It can be seen that an increase in the amount of load (stress) results in an increase in longitudinal ultrasonic velocity. These values obtained were used to draw-up tentative warning guidelines (based on uniaxial tension) to be used during underground monitoring.

When the stress on the bolts increases, the microstructure changes from non-magnetic austenite (γ) to a magnetic martensite (α') phase. The amount of martensite (α') phase increases when straining the alloy. The acoustic properties of metals and alloys are influenced by variations in structure and metallurgical condition.

Table 8. Ultrasonic sound velocity measurements of the stressed 20 mm diameter mini-bolts

Strain	Ultrasonic velocity (m/s)	%Ferromagnetic phase
0	5643	0
0.0003	5643	0.24
0.0005	5647	0.27
0.0043	5652	0.34
0.0018	5652	1.17
0.0117	5657	1.29
0.0245	5672	1.50
0.0335	5676	2.02
0.052	5678	5.34
0.075	Nd*	14.1

Nd = not determined*

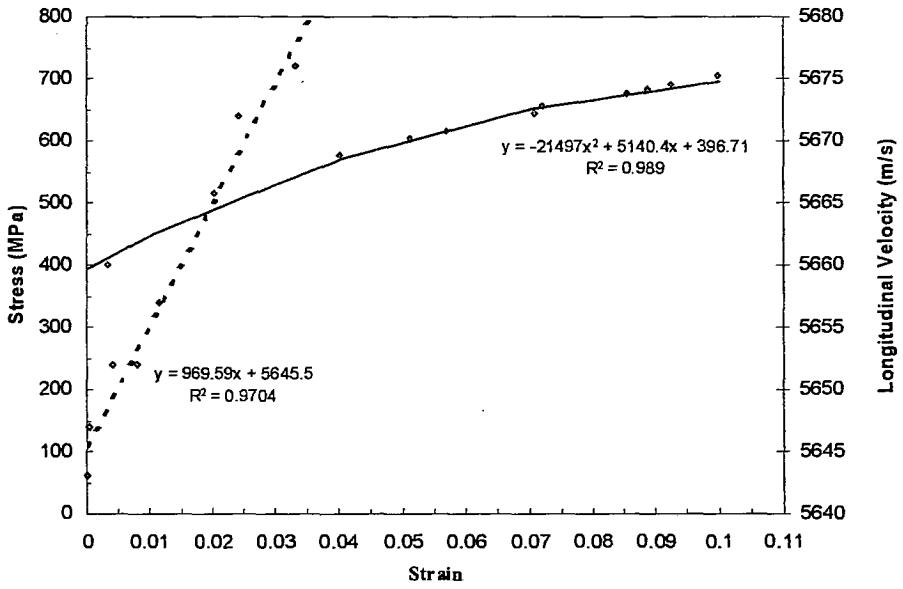

Figure 29. Velocity and stress as a function of strain of the Smartbolt™ alloy

6.4 Multiaxial Stress

6.4.1 Martensitic (α′) transformation under multiaxial stress

All working processes such as rolling, forging etc, cause plastic deformation and, consequently, these operations will involve the processes of slip or twinning or both. The stress system applied during these operations is often quite complex, but for plastic deformation to occur, the presence of a shear stress is essential. These stresses arise in most processes even when the applied stress is not a pure shear stress. A consideration of the tensile test shows that it is the shear stresses generated in the specimen, which lead to plastic deformation.

Strain-induced martensite forms as a direct consequence of plastic deformation by a mechanism distinct from athermal (spontaneous on cooling from unstressed, unstrained austenite). Martensitic embryos are formed at the intersections of microscopic shear bands during deformation. However, the martensite (α′)[51] is found in greater amounts when the loading is multiaxial compared to uniaxial due to the larger number of microscopic shear bands it creates. Loading *in situ* is not necessarily uniaxial but a mixture of tensile, shear and frictional forces.

Laboratory studies were carried out whereby multiaxial loading was simulated by cold rolling in a 2-high laboratory mill. The influence of strain on transformation was measured by a magnetic method (ferritescope). A comparison was made with uniaxial strain testing and the results are shown in Table 9. These are also graphically presented in Figure 30.

Figure 30 shows the variation in the volume fraction of martensite (α') with % reduction in thickness during room temperature rolling. It is observed that the amount of α' increases in a non-linear fashion with an increase in % reduction in thickness. It appears that the increase in the amount of α' formed per unit % reduction in thickness increases at a faster rate after about 20%. It also shows that the amount of martensite formed in this alloy increase in an almost exponential manner with increasing amount of deformation (within the range of cold working studied). The main features of microstructural developments during room temperature rolling of the Smartbolt^{TM} alloy can be speculated as follows:

- deformation of grain occurs by shear band formations
- the number of non parallel shear bands increases with increase in strain
- some of the shear band intersections become the nucleus for the α' martensite formation
- the growth of α' martensite occurs due to the increase in number of shear bands intersections as a results of increase in strain

The Smartbolt^{TM} alloy tends to behave differently during rolling as compared to tension testing. To illustrate this, a deformation of 5% results in the formation of a high amount of α' martensite during rolling/cold working compared to tension. At 5% deformation, the transformation rate during multiaxial loading is approximately 15 times more than that of uniaxial loading. Unfortunately, few measurements below 5% deformation were taken.

Table 9. % Ferromagnetism measurements of the deformed Smartbolt™ alloy

	%Ferromagnetic phase indicated by ferritescope	
Strain ($x10^{-2}$)	Uniaxial	Multiaxial
0	0	0
2	0.1	nd
5	0.3	3.9
9.8	1.2	7.0
11	1.7	8.2
12	2.0	9.5
13	2.5	10.4
14	3.5	12.1
16	4.4	14.7
20	6.1	18.5
25	8.6	28.4
30	nd	35.9
33	nd	36.4
35	nd	39.7
37	nd	42.1

nd = not determined

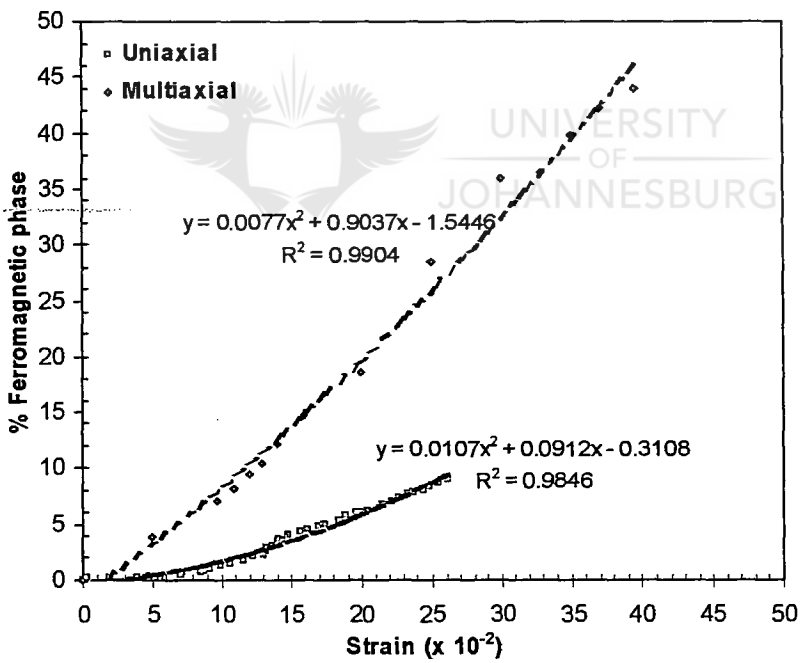

Figure 30. Percentage ferromagnetic phase as a function of strain for Smartbolt™ alloy

6.4.2 Modelling of Smartbolt™ alloy during multiaxial testing

Modelling work under multiaxial loading was also carried out to study the effect of strain (von Mises) on the kinetics of martensitic transformation. Secondly, to compare the strains and martensite obtained during uniaxial with multiaxial situations using the von Mises equivalent strain.

The transformation of metastable austenite to martensite during deformation depends on the degree of deformation. This, in turn, is a function of the strain the material has undergone on the three principal axes. Any strain state can be summed into a single parameter, the von Mises strain, which is representative of the strain state. And this strain can be related to the amount of strain-induced martensite which has formed by means of the Olsen and Cohen model[52]. The equations are as follows:

$$F = 1 - e^{-\beta\left(1-e^{-\alpha \varepsilon_{VM}}\right)^n} \qquad (13)$$

where F = fraction of martensite (i.e. $0 \leq F \leq 1$)

α, β, n = constants

$$\varepsilon_{VM} = \frac{\sqrt{2}}{3}\sqrt{(\varepsilon_1 - \varepsilon_2)^2 + (\varepsilon_2 - \varepsilon_3)^2 + (\varepsilon_3 - \varepsilon_1)^2} \qquad (14)$$

= von Mises strain

ε_1, ε_2, ε_3 = true strain in the length, width, and thickness of the material

The model produces a sigmoidal relation. The inverse relation of equation (13) is given by:

$$\varepsilon_{VM} = -\frac{\ln\left(1-\left(\frac{-\ln(1-F)}{\beta}\right)^{\frac{1}{n}}\right)}{\alpha} \qquad (15)$$

Previous work on the Smartbolt™ alloy demonstrated that there was a relation between the degree of martensite transformation and the amount of strain undergone in uniaxial tensile testing. However, recent experience has suggested that much higher amounts of martensite can form in Smartbolts, which had been installed as rockbolts underground.

Literature shows that strain-induced martensite formation is greater under multiaxial strain, and this is because of the higher degree of shear strain which occurs. In a uniaxial tensile test, $\varepsilon_2 = \varepsilon_3 \approx -\varepsilon_1/2$, and the von Mises strain is therefore $\sim\varepsilon_1$.

Under plane strain conditions, $\varepsilon_2 \approx 0$ and $\varepsilon_3 < 0$, with the result that the von Mises strain is always significantly higher than under uniaxial strain. The effect of plane strain on the Smartbolt alloy was investigated by cold rolling lengths of the material and measuring the dimension changes as well as the ultrasound velocity in the material and the martensite content. It was attempted to relate the von Mises strain to the martensite content and the ultrasound velocity under these conditions.

It must be pointed out at the outset, that cold rolling of a Smartbolt™ is not intended as a simulation of the strains imposed on an installed rockbolt. It was used to demonstrate that the empirical and theoretical steps taken to generate the models are sound and applicable to multi-axial strain situations. The actual strain state on a rockbolt can only be measured by extracting it from the rock, a time-consuming, expensive, and somewhat dangerous process. Unfortunately, the only other method available to use this data is to use data from rock mechanics models to infer the three dimensional strains in the rock bolts, and to convert these to von Mises strains, and then to determine how consistent the ultrasonic measurements are with the predictions. Such an approach is practical, but does not give absolute results; one would expect that such a model could be refined with more time and experience.

6.4.2.1 Method

Round bars of the Smartbolt alloy were cold rolled from an initial diameter of 20mm down to a rectangular cross-section with a thickness of ~12mm. The rolling was halted at this point because significant cracking (i.e. plastic instability) of the bar was occurring. Measurements of the bar dimensions – length, thickness and width – were made periodically during rolling, and the sound velocity in the bar was also measured. Also, ferritescope readings were taken at a number of positions on both sides of the bar throughout its length and averaged. The two bars (Rockbolt 1 and Rockbolt 2) tested in this manner had similar lengths of ~350mm long.

All data fitting was performed using Excel. Two methods were used for optimising the fit:

- standard polynomial regression curves were used to determine empirical relationships
- non-polynomial relationships were optimised numerically using the "Solver" routine in Excel

The "Solver" routine was used iteratively to minimise an error function (defined as the sum of the squares of the error for each prediction compared to the measured value). The heuristic used in the "Solver" routine will not alter the fitting variables (i.e. those parameters which are unknown) unless sufficient constraints on the solution are in place. This was achieved by forcing the models to predict the measured values at the lowest and highest points.

6.4.2.2 Measured Data

The data measured are shown in Tables 10 and 11, and all dimensions are given in millimetres. All of the bars were found to have the same initial sound velocity of 5645m/s. Small strains were measured in the width direction, indicating that the conditions were not truly plane strain as mentioned above. As expected, the sound velocity was found to increase as more martensite formed, and the results of the tests on separate bars were very consistent.

The strains were converted from engineering strain to true strain using the standard formula:

$$\varepsilon_1 = \ln\left(L_1/L_0\right) \quad \text{etc.}$$

It is important to note that the ferritescope readings are representative of the martensite content, but do not measure it in absolute terms. Martensite gives a different degree of magnetic saturation compared to ferrite, and therefore the ferritescope will always underestimate the martensite content.

For the Smartbolt™ alloy, ferritescope readings are known to be approximately half that of the true martensite level. To convert ferritescope readings into true martensite contents, it would be necessary to determine the latter by X-ray diffraction or possibly image analysis, and then to relate these measurements to the ferritescope readings by regression.

Table 10. Test data from Rockbolt 1

Length			Width			Thickness			Sound Velocity	Ferritescope Reading
L	#e_1	ε_1	W	#e_2	ε_2	t	#e_3	ε_3	V	100F
346.0	0.00	0.000	20.0	0.00	0.000	20.0	0.00	0.000	5645	0.0
351.8	1.68	0.017	21.2	6.00	0.058	18.0	-9.80	-0.103	5660	5.7
358.3	3.55	0.035	21.7	8.50	0.082	17.1	-14.70	-0.159	5696	13.7
367.9	6.33	0.061	21.9	9.50	0.091	16.1	-19.30	-0.214	5705	20.6
383.3	10.78	0.102	22.0	10.00	0.095	15.1	-24.45	-0.280	5709	28.2
394.6	14.05	0.131	22.0	10.10	0.096	14.0	-30.00	-0.357	5711	36.4
410.8	18.73	0.172	22.0	10.00	0.095	13.1	-34.75	-0.427	5748	41.7
424.5	22.69	0.204	22.1	10.50	0.100	12.2	-39.00	-0.494	5774	44.3

F is the fraction of martensite; 100F is the percentage martensite
#$e_{1,2}$ is the % elongation and #e_3 % reduction

Table 11. Test data from Rockbolt 2

Length			Width			Thickness			Sound Velocity	Ferritescope Reading
L	#e_1	ε_1	W	#e_2	ε_2	t	#e_3	ε_3	V	100F
350.6	0.00	0.000	20.0	0.00	0.000	20.0	0.00	0.000	5645	0.0
352.2	0.46	0.005	20.0	0.00	0.000	19.0	-5.00	-0.051	5649	3.9
356.9	1.80	0.018	21.2	6.00	0.058	18.0	-9.80	-0.103	5666	7.0
359.2	2.45	0.024	21.7	8.50	0.082	17.8	-11.00	-0.117	5668	8.2
360.0	2.68	0.026	21.7	8.50	0.082	17.6	-12.00	-0.128	5679	9.5
360.5	2.82	0.028	21.8	9.00	0.086	17.4	-13.00	-0.139	5680	10.4
361.5	3.11	0.031	21.8	9.00	0.086	17.2	-14.00	-0.151	5683	12.1
367.5	4.82	0.047	22.0	10.00	0.095	16.8	-16.00	-0.174	5697	14.7
373.0	6.39	0.062	22.0	10.00	0.095	16.0	-20.00	-0.223	5706	18.5
386.0	10.10	0.096	22.1	10.25	0.098	15.0	-25.00	-0.288	5709	28.4
401.2	14.43	0.135	22.1	10.25	0.098	14.0	-30.00	-0.357	5712	35.9
408.2	16.43	0.152	22.2	10.75	0.102	13.4	-33.00	-0.400	5725	36.4
415.7	18.57	0.170	22.2	10.75	0.102	13.0	-35.00	-0.431	5750	39.7
421.8	20.31	0.185	22.2	11.00	0.104	12.6	-37.00	-0.462	5762	42.1
431.3	23.02	0.207	22.2	11.00	0.104	12.1	-39.50	-0.503	5780	44.0

F is the fraction of martensite; 100F is the percentage martensite
#$e_{1,2}$ is the % elongation and #e_3 % reduction

6.4.2.3 Relation of Martensite Content to von Mises Strain

Using the Olsen and Cohen model[52], the following equation was found to give the best fit for the rockbolt data. The curve along with the data it models is plotted in Figure 31.

$$F = 1 - e^{-0.846\left(1 - e^{-4.63\,\varepsilon VM}\right)^{2.58}} \quad (16)$$

i.e. $\alpha = 4.63$, $\beta = 0.846$ and $n = 2.58$

No attempt has been made here in this work to compare the values obtained for these constants with values in the literature for other alloys. Figure 31 may imply that the Smartbolt™ alloy displays some stress-induced martensite (curve cross the y-axis above the origin) but there are insufficient data points to confirm if this is indeed the case.

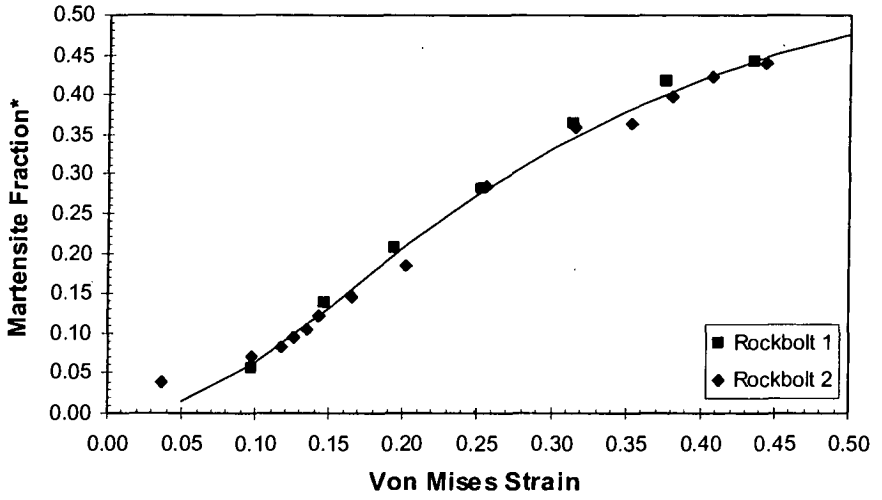

Figure 31. Olsen and Cohen model applied to data from Rockbolts 1 and 2
** Ferritescope reading as a fraction rather than percent*

Data from a uniaxial test, (see Figures 25 and 26, and Table 12) in which ferritescope and velocity readings but no area reduction measurements were made, was modelled in a similar fashion. Since there is a phase change, it is incorrect to assume that the volume is constant during plastic deformation. However, since the volume change is relative small, such an assumption can allow one to calculate first approximations of the minor strains. In a unaxial tensile test, the minor strains should be equal, and if the volume is constant, it can be shown that:

$$e_2 = e_3 = \frac{-\left(1+e_1-\sqrt{1+e_1}\right)}{1+e_1} \qquad (17)$$

where e_1, e_2, e_3 = engineering strain and are expressed as fractions rather than percentages

Table 12. Uniaxial test data processed as described in Section 6.4.2.1

Length			Diameter			Von Mises ε	α' Fraction	Sound Velocity
L	e_1	ε_1	W	e_2	ε_2	ε_{VM}	F	V
2400.0	0.00	0.000	20.0	0.00	0.000	0.000	0.000	5640
2400.7	0.03	0.000	20.0	-0.01	0.000	0.000	0.002	5643
2401.2	0.05	0.000	20.0	-0.02	0.000	0.000	0.003	5647
2410.3	0.43	0.004	20.0	-0.21	-0.002	0.004	0.003	5652
2419.4	0.81	0.008	19.9	-0.40	-0.004	0.008	0.013	5652
2428.1	1.17	0.012	19.9	-0.58	-0.006	0.012	0.012	5657
2458.8	2.45	0.024	19.8	-1.20	-0.012	0.024	0.015	5672
2480.4	3.35	0.033	19.7	-1.63	-0.016	0.033	0.020	5676
2524.8	5.20	0.051	19.5	-2.50	-0.025	0.051	0.053	nd
2580.0	7.50	0.072	19.3	-3.55	-0.036	0.072	0.145	nd

nd = not determined

Table 12 shows the data processed using equation 17, expressed in terms of a hypothetical 2.4m rockbolt. Figure 32 shows that the uniaxial data agrees with the model developed for Rockbolt 1 and 2 when the von Mises effective strain is used to construct the graph as compared to Figure 30 where the data is constructed using engineering strain. Thus Figure 32 shows that the Olsen-Cohen model together with the von Mises effective strain replacing the uniaxial strain, produces a fair prediction for the kinetics of the martensitic transformation in the Smartbolt alloy under a complex multiaxial strain state.

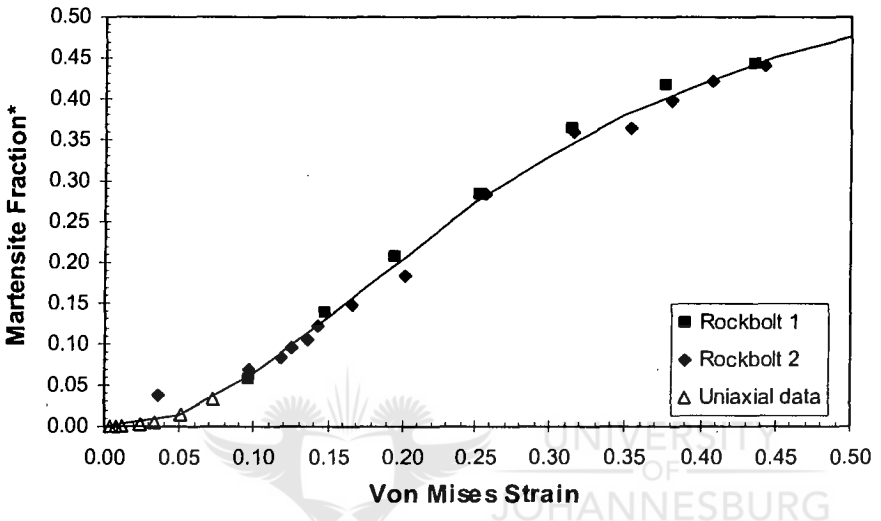

Figure 32. Olsen and Cohen model applied to data from Rockbolts 1 and 2, compared to estimate of data from uniaxial tensile test
** Ferritescope reading as a fraction rather than percent*

6.4.2.4 Relation of Martensite Content to Sound Velocity

As discussed, the sound velocity in the rockbolts depends on the amount of martensite present and this is shown in Figure 33. The first section of the curve (labelled 1) shows a substantial increase in sound velocity probably because of the rapid increase in martensite content, which then becomes constant over a relatively short region (labelled 2) and finally increases until martensite saturation is approached. This region is associated with voids formation and cracking. The volume percentage of martensite in the first section of the curve is linearly related to sound velocity and this region is the most useful for assisting with the task of monitoring an installed Smartbolt™.

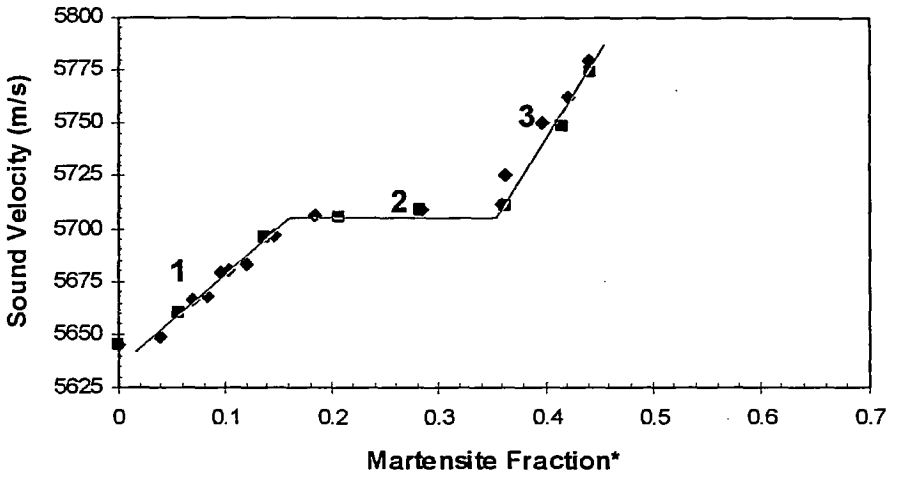

Figure 33. Ultrasonic sound velocity as a function of martensite fraction data for Rockbolts 1 and 2
** Ferritescope reading as a fraction rather than percent*

The ferritescope reading, which corresponds to a "fully" martensitic microstructure, can never be "100%" (as discussed in Section 6.4.2.2). Furthermore, the maximum level of martensite (i.e. saturation of the austenite with martensite) occurs at a martensite volume fraction lower than 1, and this level depends on the chemistry, *inter alia*. The ferritescope reading that corresponds to a slow down in the martensite formation rate (i.e. the constant section of the curve) is 35.5%, and the corresponding (critical) ultrasonic velocity is ±5711m/s. Another, more empirical method of determining "critical" velocity (warning guidelines) shown in Appendix A.

This condition of the Smartbolt™ alloy would be expected to be associated with the onset of cracking – there is insufficient austenite present to accommodate further plastic deformation, and instead it is the inherent ductility (or lack thereof) of the martensite which must do so. Thus the velocity and the martensite content both can be used to determine when the bolt is close to failure.

In summary it has been demonstrated that the acoustic measurements have a complex dependence on the multiaxial strain state, and therefore more knowledge of this strain state is required. Such knowledge for installed rockbolts may be obtained by interrogating rock mechanics models, which are, used by mine rock engineers.

6.5 Testing on the mine

To test and demonstrate the effectiveness of the Smartbolt technology, a test site was identified and prototype roofbolts were installed in two different sections of a South African gold mine, (see section 5.4). Loosening of rockbolt anchors after blasting, appears to be a major problem in most of the mines where conventional mining is taking place. This is due to the current tensioning method, which is generally done manually with a simple tool such as a spanner. It was therefore agreed with the mine personnel, to install the Smartbolts, using both chemical (cement) and expansion shells and to use a torque wrench for pre-tensioning of the bolts (to a value of ±35Nm).

In many situations underground, the bolt is not in pure tension, but more usually a combination of tension, shear, etc. Allowance must be made for multiaxial loading conditions, as the transformation characteristics of the smartbolt alloy are different in this case. Uniaxial tension produces less martensite compared to the multiaxial state under the same experimental condition, due to multiple slip systems being activated in multiaxial loading. The warning guidelines that are shown in Table 13 were constructed based on the work carried out in sections 6.3.1 and 6.4 and they were used to interpret the readings from underground monitoring.

Structural health monitoring in underground facilities and especially in haulage tunnels used in South African deep gold mines is an extremely important engineering problem and is of paramount importance due to safety reasons.

The rationale behind ensuring the integrity of tunnels openings and safety of personnel using these tunnels is clear: avoiding danger as potential injuries to personnel (as well as the significant financial losses incurred in rehabilitating tunnels) after an accident cannot be tolerated by any of the affected parties.

Large stresses are present in the surrounding rockmass, which cause the tunnels to close up over time. As the tunnels become more stressed and accumulate damage, they represent a greater threat to the safety of those working in these tunnels. The current support systems used in these tunnels also become over-stressed and damaged over time. Consequently, they cannot withstand rockfalls, rockbursts and seismically induced rockmass movements.

On the basis of Smartbolt technology, it is possible to assess deformations as well as to track the appearance and propagation of cracks in the sides of tunnels. Also, using this technology, it is possible to measure the stresses experienced by the surroundings. Fourteen Smartbolts were installed in a haulage tunnel to monitor the stresses that are experienced in that area. These Smartbolts were monitored (interrogated with an ultrasonic device) over a period of twelve months to see if there was any structural change.

The results obtained during the fieldwork are summarised in Table 14 and graphically presented in Figure 34. Almost 50% of the installed Smartbolts are experiencing a significant increase in stress. Also, some of the bolts have developed a monotonic pattern of increasing load with time. Installed bolt-number 84, showed to have experienced a high stress as compared to the other bolts. With continued mining in the vicinity of this area, it is anticipated that further increases in load/stress will be measured. At present, mining is taking place in level 93, which is just above this section.

Another twenty Smartbolts were installed at the ramp of a haulage tunnel. However, these were only monitored over a period of seven months. Their results are summarised in Table 15 and graphically presented in Figure 35. Some of the Smartbolts show a pattern of gradual increase in stress but not as high as in the previous section. This may be due to the fact that no mining is currently taking place near or at this area; it is planned by the mine personnel to start mining in the next few months. It is therefore anticipated that the bolts will experience large stresses as mining takes place in that area.

Table 13. Potential Smartbolt warning guidelines

Ultrasonic sound velocity (m/s) (uniaxial)	**Ultrasonic sound velocity (m/s) (multiaxial)**	**Comments**
5640 to 5652	5640 to 5676	Stresses in elastic range
5652 to 5672	5676 to 5715	Bolt is yielding
>5672	>5715	Bolt is showing substantial plastic deformation

Table 14. Summary of the ultrasonic sound velocity results of Smartbolts installed at a South African gold mine (94L Haulage no. 2)

	Dimensions	**Ultrasonic sound velocity (m/s)**								
Bolt number	Length x diameter (mm)	*29/10/03*	*04/11/03*	*25/11/03*	*20/01/04*	*29/01/04*	*19/03/04*	*02/04/04*	*03/05/04*	*07/09/04*
54	2400 x 20				5640	5649	5698	5698	5698	#
59	2400 x 20	5641	5642	5642	5642	5642	5642	5642	#	5684
62	2400 x 20	5641	5642	5656	5661	5661	5663	5665	#	5692
66	2400 x 20	*	*	*	5640	5651	5712	5717	#	5734
72	2400 x 20	*	*	*	5640	5651	5686	5686	5689	5703
75	2400 x 20	*	*	*	5640	5644	5647	5677	5689	#
76	2400 x 20	*	*	*	5640	5654	5661	5661	5663	#
85	2400 x 20	5640	5642	5656	5670	5672	5673	5726	5766	5774
86	2400 x 20	*	*	*	5640	5647	5682	5682	#	#
90	2400 x 20	*	*	*	5640	5654	5698	5700	5700	#
92	2400 x 20	5640	5649	5649	5649	5649	5651	5677	#	5683
94	2400 x 20	*	*	*	5640	5651	5651	5658	5665	5677
96	2400 x 20	*	*	*	5640	5649	5658	5684	5684	#

** → bolts not installed*

 # → measurements were not taken

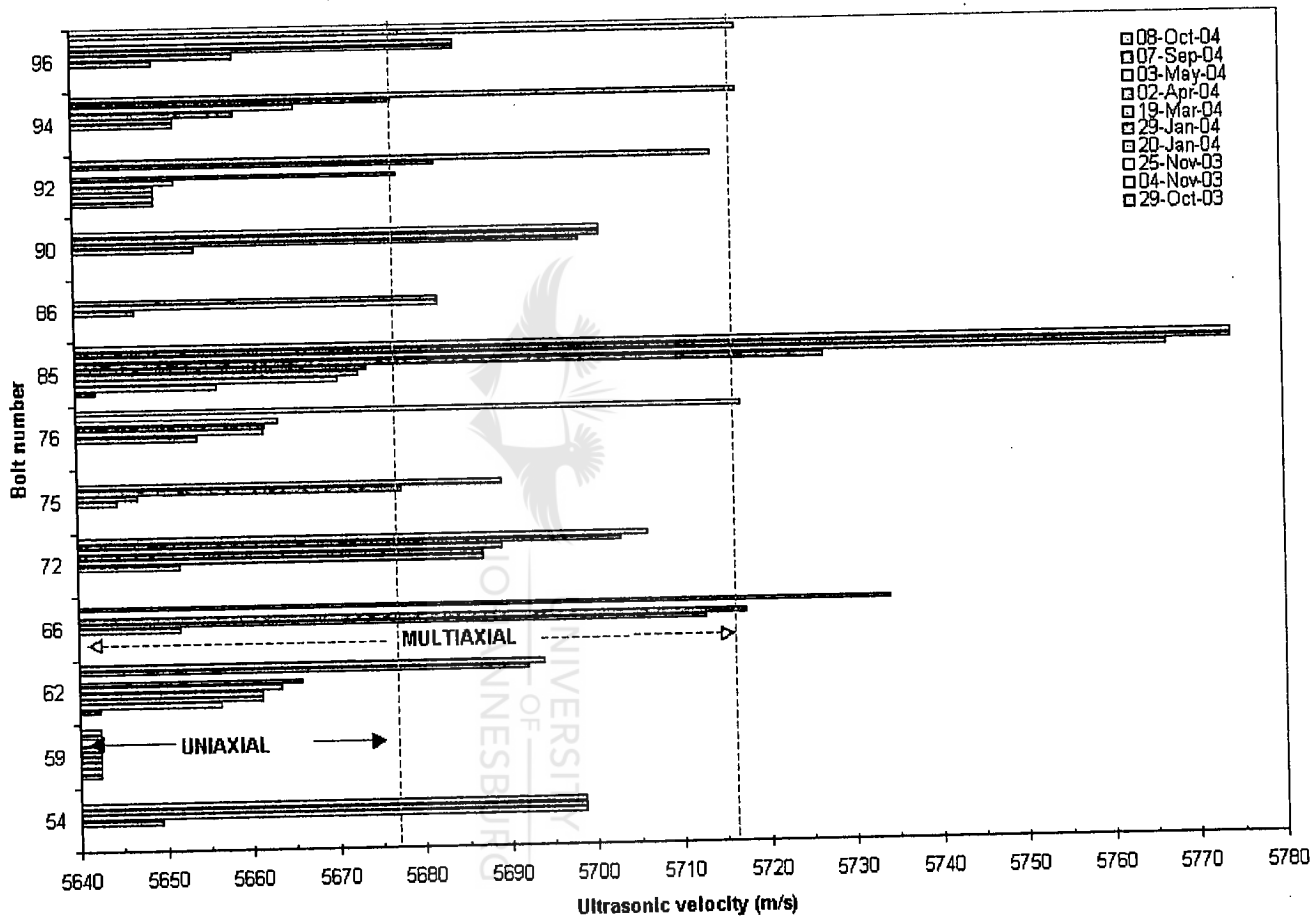

Figure 34. Graphical presentation of the results obtained from a South African gold mine (94L no. 2 Haulage)

Table 15. Summary of the ultrasonic sound velocity results of smartbolts installed at a South African gold mine (94L Haulage ramp)

	Dimensions	Ultrasonic sound velocity (m/s)				
Bolt number	Length x diameter (mm)	*17/03/2004*	*19/03/2004*	*02/04/2004*	*03/05/2004*	*07/09/2004*
51	2400 x 20	5644	5644	5661	5661	5680
52	2400 x 20	*	5645	5645	5640	5678
56	2400 x 20	*	5640	5640	5640	5680
58	2400 x 20	*	5640	5640	5640	5661
60	2400 x 20	*	5640	5640	5640	5673
67	2400 x 20	*	5640	5640	5640	5647
70	2400 x 20	5644	5644	5656	5656	5680
73	2400 x 20	*	5640	5640	5640	5642
74	2400 x 20	*	5640	5640	5640	5645
77	2400 x 20	*	5640	5640	5640	5647
78	2400 x 20	5652	5652	5654	5684	5687
80	2400 x 20	*	5642	5642	5640	5675
81	2400 x 20	*	5640	5640	5640	#
82	2400 x 20	*	5640	5640	5640	5682
87	2400 x 20	*	5640	5640	5640	5682
88	2400 x 20	*	5640	5640	5640	5675
93	2400 x 20	*	5640	5640	5640	5675
97	2400 x 20	5647	5647	5647	5647	5647
98	2400 x 20	*	5640	5640	5640	5649
100	2400 x 20	*	5640	5640	5640	5687

* → *bolts not installed*

\# → *measurements were not taken*

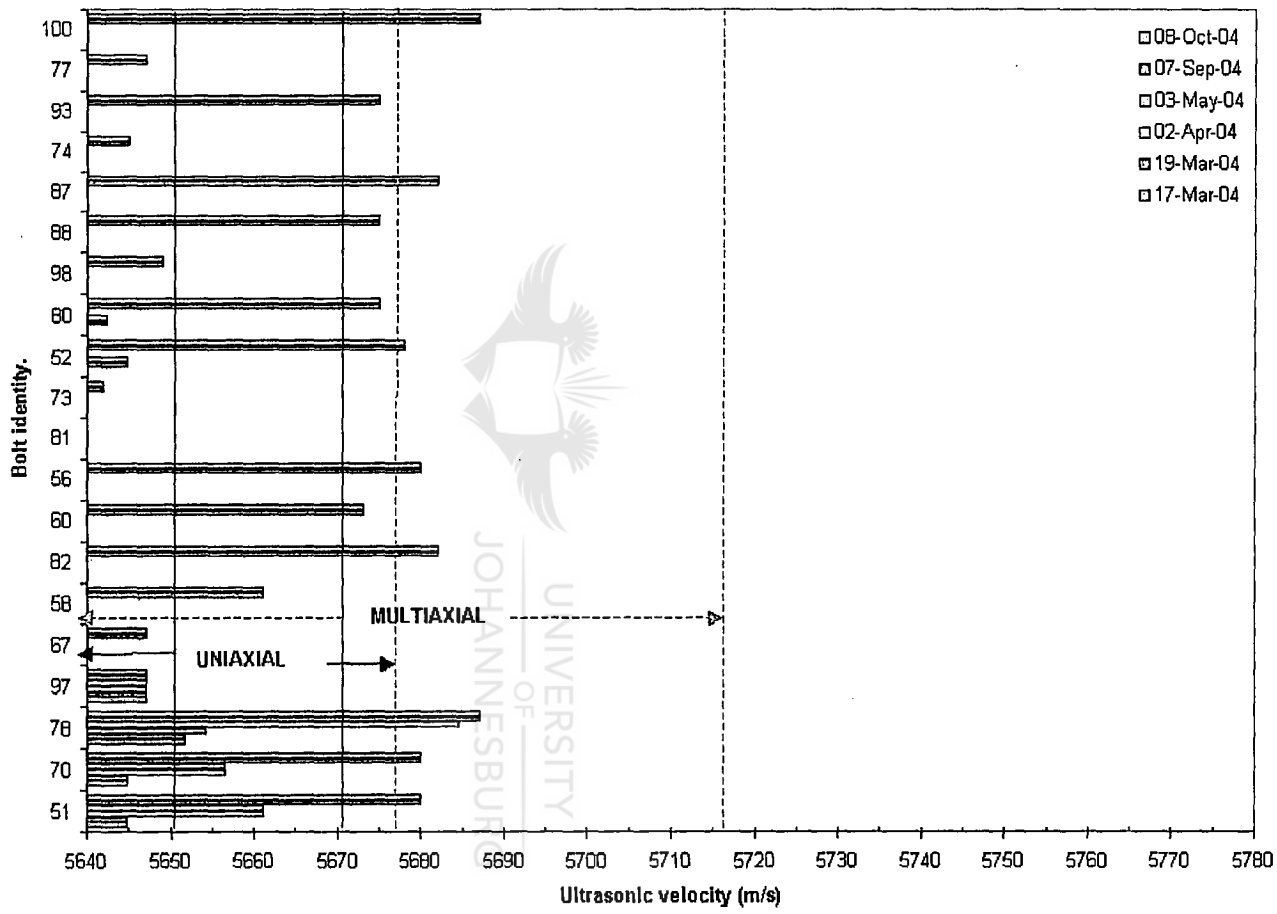

Figure 35. Graphical presentation of the results obtained from a South African gold mine (94L Haulage ramp).

CHAPTER 7

7 Conclusions

The following conclusions can be drawn from this study:

- An alloy composition has been identified as being suitable for acting as a Smartbolt material under the influence of strain. From the experimental work, it was found that the Smartbolt™ alloy could be used as a strain monitors in rockbolt applications.
- The use of the Smartbolt concept together with ultrasonic monitoring can be an effective and simple method of monitoring the load in a bolt. The readings are accurate and the technique should help to promote safety in the industry. Information can be gathered and logged quickly to determine whether bolts are bent, broken, or overloaded.
- Ultrasonic methods appear to be a satisfactory method for interrogating Smartbolts but the overall hardware package may need to be refined with continuing feedback from mining personnel. A more simple and cheaper device would be advantageous.
- It was demonstrated that acoustic measurements have a complex dependence on the multiaxial strain state, and therefore more knowledge of this strain state is required. Such knowledge for installed rockbolts may be obtained by interrogating rock mechanics models, which are, used by mine rock engineers.
- The installed Smartbolts (in 94 Level no. 2 haulage and haulage ramp) interrogated with an ultrasonic device over a period of twelve and six months respectively, showed a monotonic pattern of increasing load with time.
- Based on the outcome of the field test results, the Smartbolt technology would be more suitable in reducing the incidence of rockfall as compared to rockbusrt.
- The Smartbolts are installed along the standard carbon steel bolts to act as strain monitoring device and to complement each other.

CHAPTER 8

8 References

1 Moema, J.S., Paton, R., Roberts, S. and Adams, D. Smartbolt Technology and Methods of Monitoring, to Assess the Condition of Mining Roof Support systems. *7th International Colloquium on Asset Management of Aged Plant and Materials Assessment Methods,* Cape Town, South Africa, (2003) p153-167.

2 Paton, R., Moema, J., Fletcher, C.J. and Adams, D. The use of smartbolt technology to assess the condition of mining roof support system. *6th International Colloquium on Aging of Materials And Methods For The Assessment And Extension Of Lifetimes Of Engineering Plant,* Cape Town, South Africa, (2001) p39-51.

3 Chopra, I., Review of State of Art of Smart Structures and Integrated Systems, *American Institute of Aeronautics and Astronautics, AIAA Journal* (USA), vol. 40, no. 11, pp 2145-2187, Nov. 2002.

4 Reddy, J.N., and Cheng, Z.Q., Three Dimensional Solutions of Smart Functionally Graded Plates, *Journal of Applied Mechanics (Transactions of the ASME),* (USA), vol. 68, no. 2, pp 234-241, Mar. 2001.

5 Stacey, T.R., Reliable Cost Effective Technique for *in-situ* Ground Stress Measurements in Deep Gold Mine, *SIMRAC Report, GAP 220*, Fundamental and Applied Research, Jul. 1995.

6 Gay, N.C., Conceptual Development of a Method to Determine the Principal Stress around Coal Mine Working to Ensure Safe Mine Design, *SIMRAC Report, COL 326*, Fundamental Research, 1998

7 Canbulat, I., and Jack, B.W., Review of Current Design Methodologies to improve Safety of Roof Support Systems, Particularly in the Face Area, in Collieries, *SIMRAC Report, COL 328*, Strata Control, Dec. 1998.

8 Stacey, T.R., and Wesseloo, J., Application of Indirect Stress Measurement Techniques (non strain gauge based technology) to Quantify Stress Environment in Mines, *SIMRAC Report, GAP 858*, Applied Research, Mar. 2001.

9 Leng, J.S., and Asundi, A., Non-Destructive Evaluation of Smart Materials by using Extrinsic Fabry-Perot Interferometric and Fiber Bragg Grating Sensor, *NDT & E International (UK), vol. 35,* no. 4, pp 273-276, 1 Jun. 2002.

10 Murayama, H., Kageyama, K., Naruse, H., Shimada, A., and Uzawa. K., Structural Health Monitoring by Using Fiber-Optic Sensor for Large Composite Structures, *Journal Of the Japan Society for Composite Materials (Japan),* vol. 28, no.5 pp 176-188, 2002.

11 DTI Stress....web site: http://www.smartbolts.com., accessed on 2004.

12 Altounyan, P., and Taljaard, D., Developmens in controlling the roo in South African coal mines-a smarter approach., Coal- *The Future, 12th International Conference on Coal Research*, South African Institute of Mining and Metallurgy, 2000.

13 Altounyan, P., and Minney, D., Field Experience of Measuring The Acoustic Energy from a Hammer Blow to Coal Mine Roof and its Relationship to Roof Stability., *19th Conference on Ground Control in Mining Lakeview Resort and Conference Centre, August*, 2000.

14 Rockburst....web site: http://www.deepmine.csir.co.za accessed on 2004

15 Wood, H.E., The Witwatersrand earth tremors, *J. Chem. Metall. Mining Soc. of SA*, vol. 14, pp. 423-427, 1914.

16 Allen, W., Notes on recent observations of remnants, *J. Chem. Metall. Mining Soc. of SA*, XXXII, pp. 1-5, 1931.

17 Weiss, O., The Theory of rockbursts and the possibilities of geophysical methods in predicting rockbursts on the producing mines of the Witwatersrand, *J. Chem. Metall. and Mining Soc. of SA*, vol. 38, pp. 273-329, 1938.

18 Morrison, R.G.K., A general theory of rockbursts, *Eng. and Mining J.. Part II*, vol. 149, pp. 68-70, 1948.

19 Spalding, J., Observation on rockbursts, *Engng. and Mining J.*, vol. 149, pp. 91-93, 1948.

20 Hill, F.G., An investigation into the problem of rockbursts. An operational research project, *J. Chem. Metall. and Mining Soc. of SA*, pp. 63-83, Oct and Nov 1954.

21 Cook, N.G.W., Jaeger, J.C., Rock mechanics applied to the study of rockbursts, *J.S.A. Inst. Min. and Metall.*, pp. 435-528, discussion pp 695-714., 1954.

22 Brink A.v.Z. and O'Conner D.M., Research on the prediction of rockbursts at Western Deep Levels, *J.S.A. Min. Metall.*, vol. 38, pp. 1-10, 1954.

23 Salamon, M.D.G., Rockbursts hazard and the fight for its alleviation in South African gold mines, *in: Rockbursts: Prediction and Control, Inst. of Min. and Metall, London,* pp. 11-36, 1983.

24 Cook, N.G.W., Origin of Rockburst, in Rockburst: Prediction And Control, Inst. Min. and Metall, London, pp1-9, (1983).

25 Gay N.C., Spencer D., van Wyk J.J. and van der Heever P.K., The control of geological and mining parameters in the Klerksdorp gold mining district, *proc: 1st Int. Congress on Rockbursts and Seismicity in Mines*, (eds: N.C Gay and E.H. Wainwright), Johannesburg, 1982, SAIMM, pp. 107-120,1984.

26 Ortlepp W.D., An overview of a problem in South African and a comparison with some rockbursts at El Teniente mine, *A.A.C. Gold and Uranium Div. report 014/23 April 1990.*

27 Knoll P. and Kuhnt W. Seismological and technical investigations of the mechanics of rock bursts, in: *Rockbursts and Seismicity in Mines,* (ed: C. Fairhurst), Balkema, Rotterdam, pp 129-138, 1990.

28 Johnston J.C. and Einstein M.H., A survey of mining associated seismicity, in: *Rockbursts and Seismicity in Mines,* (ed: C. Fairhurst), Balkema, Rotterdam, pp 121-125, 1990.

29 King C-Y., Multicycle slip distribution along a laboratory faults, *Geophys. Res,* vol.96, pp 14,377-14,381, 1991.

30 Ortlepp W.D., Note on fault slip motion inferred from a study of micro-cataclastic particles from an underground shear rupture, *unpublished material, 1992.*

31 Australian proposal., http://www.acg.uwa.edu.au., accessed on 2003.

32 Chamber of Mines of South Africa., The contribution of the mining and minerals industry to sustainable development in South Africa....web site: http://www.bullion.org.za., accessed on 2003.

33 Paton R., Moema J. and Fletcher CJ., Development of a sensor material using Austenitic Stainless Steel, *Mintek Confidential Communication C2891M*, Randburg, (1999).

34 Kerr, J., Du Preez, G., Paton, R., Development of an Economic Duplex Stainless Steel: *Progress Report 2, Mintek Confidential Communication C2879M*, Randburg (1999).

35 Hull, F. C., Delta ferrite and martensite formation in stainless steels, *Welding Research Supplement: Welding Journal*, (1973) May pp. 193s-203s.

36 Angel, T., Transformation of martensite in austenitic stainless steels, *Journal of the Iron and Steel Institute*, vol. 177 (1954) pp. 165-174.

37 Pickering, R.B., Physical Metallurgy and the Design of Steel., *Applied Science* Publishes Ltd, London, 1078., pp229.

38 Nohara K., Hidaka H., Pelizzetti N., Serpone N.,. Cryogenic Structural Stainless Steels., Journal of Iron and Steel Institute of Japan, 63., (1973), 5, pp212.

39 Reissner, J., and Mulders, H., New Methods for the Prediction of Formability of Stainless Steel Sheets, *Proceedings of International Conference on Stainless Steels*, Chibe, Japan, pp779, (1991).

40 Reed, R. P., Austenitic stainless steels with emphasis on strength at low temperatures, *Alloying*, J. L. Walter (ed.), M. R. Jackson (ed.), C. T. Sims (ed.), pp. 225-256, ASM International, USA (1988).

41 Talyan, V., Wagoner RH., and Lee JK., Formability of Stainless Steel, *Metallurgical and Materials Transactions A*, vol. 29A, August 1998., pp2161-2172.

42 Hecker, S.S., Stout, M.G., Staudhammer, K.P., Smith, J.L., Effect of Strain State and Strain Rate on Deformation- Induced Transformation in 304 Stainless Steel: Part I. Magnetic Measurements and Mechanical Behaviour, *Metallurgical Transactions A, vol. 13A*, April 1982, pp619-626.

43 Zackay, V., E. Parker, D. Fahr and R. Busch., The Enhancement of Ductility in High Strength Steels, *Trans. of ASM*, 60, pp. 252-259, 1967.

44 Doege, E., Kulp, S., and Sunderkotter C., Properties and Application of TRIP-steel in sheet metal forming, Steel *Research 73 (2002)* no. 6 & 7., pp303-307.

45 Vasilakos A.N., Ohlert J.; Giasla, K.; Haidemenopoulos G.N., and Wolfgang B., Low-alloy TRIP steels: a correlation between mechanical properties and the retained autenite stability., *Steel Research 73 (2002)* no. 6 & 7., pp249-252.

46 ASTM E8-99., *Test Method for Testing Testing of Metallic Materials*, American Society for Testing and Materials, West Conshohocken, USA, 2000.

47 ASTM E494-75., Standard Practice for Measuring Ultrasonic Velocity in materials, *American Society for Testing and Materials*, West Conshohocken, USA, 2000.

48 USM 25, Technical Reference and Operating Manual., *Krautkramer., EN 12668-1.*

49 Bressanell, J.P., and Moskowitz A., *Martensite and Deformation Twinning in Martensite Steels.*, Trans. ASM, 54, (1966), 223.

50 Ludwigson, D. C. and Berger, J. A., Plastic behaviour of metastable austenitic stainless steels, Journal of The Iron and Steel Institute, (1969) 413 – 419.

51 Shrinivas, V., Varma, S.K., and Murr, L.E., Talyan., Deformation Induced Martensite Characteristics in 304 and 316 Stainless Steels during Room-Temperature Rolling, Metallurgical and Materials Transactions A, vol. 26A, March 1995., pp661.

52 Olsen, G.B., and Cohen, M., *Kinetics of Strain Induced Martensite Nucleation.*, Metallurgical Transactions *A, vol. 6A*, 1975, p 791.

Appendix A

A. Empirical method of determining critical velocity (warning guidelines)

Ultrasonic sound velocity and % ferromagnetic phase data in section 6.3.2, Table 8, obtained from uniaxial testing was used to construct initial warning guidelines. These guidelines were purely based on uniaxial conditions and conservative estimates.

In underground environment loading *in situ* is not necessarily uniaxial but a mixture of tensile, shear and frictional forces. Therefore, a preliminary laboratory simulation was carried out whereby multiaxial loading was simulated by cold rolling in a 2-high laboratory mill. The influence of strain on transformation was measured with a magnetic method (ferritescope). The % ferromagnetic phase and strain test data obtained from this work is summarised in section 6.4, Table 9 and graphically presented in Figure 36. Two points (% ferromagnetic phase values) from uniaxial curve were selected and correlated to that on multiaxial curve.

A graph of ultrasonic velocity against % ferromagnetism based on uniaxial loading was plotted. It was regression fitted with a straight line and extrapolated to allow for a multiaxial loading scenario (see Figure 37). It is assumed here that there is a linear relationship between ultrasonic and ferritescope readings. This graph was then used to construct set of warning guidelines, which are shown in Table 16. They were used to interpret the readings obtained from underground during a Smartbolt monitoring session.

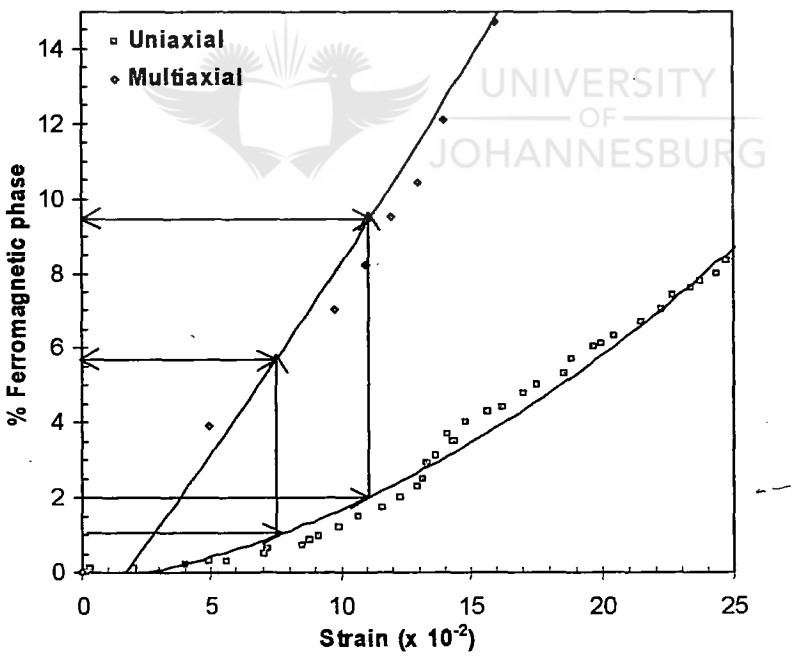

Figure 36. Percentage ferromagnetic phase as a function of strain for Smartbolt alloy

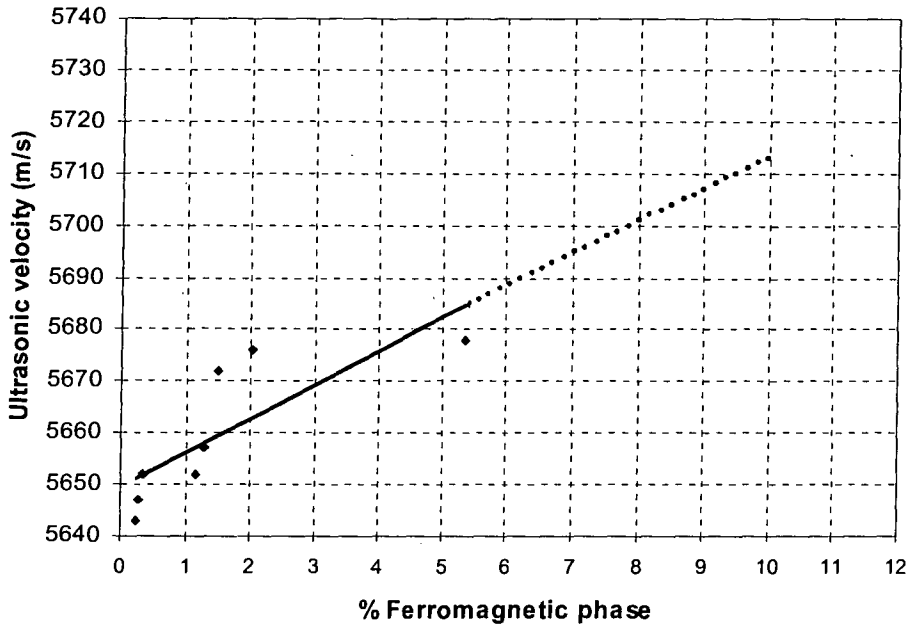

Figure 37. Variation of sound velocity with %ferromagnetic phase

Table 16. Tentative Smartbolt warning guidelines

%Ferromagnetic phase		Comments	Ultrasonic sound velocity (m/s)	
uniaxial	multiaxial		uniaxial	multiaxial
<1	<5	Stresses in elastic/plastic range	5640 to 5652	5640 to 5676
1-2	5-10	Bolt is yielding	5652 to 5672	5676 to 5715
>2	>10	Bolt is showing substantial plastic deformation	>5672	>5715